

# ValerieX (VXXX)

## A Symmetry-Based Reorganisation of Classical Buoyancy and Added-Mass Behaviour

*Density-State Disequilibrium, Valerie's Law, and the Density-State Drive*

Nicholas Parkyn

Independent Researcher

nikparkyn@googlemail.com

May 2026 v1.9.3

### Reader's Quick-Start

ValerieX does not introduce a new force or contradict classical mechanics. All governing equations are mathematically identical to the established buoyancy and added-mass framework.

What is new is the structural organisation:

- A single bounded contrast variable.
- A unified motion law:  $a = g\chi$ .
- A clear separation of drive (density contrast), coupling (geometry via  $C$ ), and resistance (drag).
- A regime-based interpretation of how motion is realised.

The contribution of ValerieX is therefore organisational and interpretive, not a replacement of existing equations.

## Abstract

ValerieX (VXXX) is a symmetry-based, motion-first reorganisation of classical buoyancy and added-mass behaviour into a unified framework based on density-state disequilibrium between substance and its surrounding environment. It does not deny classical mechanics or Newtonian gravitation and is fully consistent with the recognised buoyancy-plus-added-mass family of fluid mechanics (Lamb, 1932; Brennen, 1982; Kelvin, 1871). Its contribution is structural: a single bounded contrast variable, a clean drive/coupling/resistance separation, and a regime-based reading of how the same density-state drive is realised under different pathway conditions.

The bounded contrast variable  $\chi = (\rho_o - \rho_m)/(\rho_o + \rho_m)$  is shown to be the unique lowest-degree rational form satisfying four foundational conditions; every higher-degree rational solution factors through it. Valerie's Law  $a = g\chi$  follows by minimal sufficiency. Geometry enters through the participation coefficient  $C$  of the classical added-mass family: the bounded form is recovered exactly at  $C = 1$  (cylinder  $\perp$  axis), and the same family recovers  $C = 0.5$  for spheres in inviscid potential flow. The bounded form is therefore a specific member of standard added-mass fluid dynamics rather than an alternative to it.

Realised motion is organised by three operationally distinct regimes — constrained, supported, and unconstrained — each defined by a single observable pathway condition. The same  $\chi$  can appear as a scale reading, as tension in a support, or as realised acceleration depending on which regime applies. Together,  $\chi$ , the C-family, and the regime classification form a single motion-engine identity. ValerieX does not introduce a new measured force; it identifies a single motion-engine structure beneath the recognised equations, with density-state disequilibrium supplying the available drive, geometry setting early-time coupling through  $C$ , drag setting later realised

motion, and pathway availability determining whether the drive appears as acceleration, tension, or weight.

The framework is testable. Targeted early-time measurements at  $\rho_o = 2\rho_m$  separate the C-branches by experimentally accessible margins ( $a = 2g/5$  for spheres at  $C = 0.5$ ,  $a = g/3$  for cylinders  $\perp$  axis at  $C = 1$ ); a continuous capsule  $C(L/D)$  curve derived from prolate-spheroid added-mass theory converts shape-controlled tests into a continuous-parameter falsification target; and McKee and Czarnecki (2019) supply a positive published anchor for the  $C = 0.5$  sphere branch. ValerieX is scope-limited to vertical-motion phenomena observable under everyday and laboratory conditions; it does not address orbital, planetary, or cosmological scales, and does not derive  $g$ . Full validation requires new controlled measurements.

## Keywords

ValerieX; Valerie’s Law; density-state disequilibrium; density-state drive; bounded contrast; participating medium load; vertical motion; weight; buoyancy; terminal velocity; pathway availability; regime classification; C-family; electromagnetic field; symmetry-based reorganisation; falsifiability.

## Note on Volume Structure

This manuscript is the consolidated, read-first paper for the ValerieX framework. Cross-references in the body to Volumes I–IV (cited as Parkyn 2026a–d in the references) appear throughout as V1, V2, V3, and V4 with section numbers, directing readers to supporting technical detail in the four-volume programme: V1 — theory and derivation; V2 — regime classification and experimental discrimination; V3 — computational modelling, discriminators, and figure framework; V4 — experimental protocol and laboratory manual.

## Notation

Symbol	Meaning
$\rho_o$	Density-state of the object ( $\text{kg m}^{-3}$ )
$\rho_m$	Density-state of surrounding medium ( $\text{kg m}^{-3}$ )
$\Delta\rho$	Density-state difference, $\rho_o - \rho_m$
$\chi$	Bounded density-contrast variable, $-1 < \chi < 1$
$r$	Density ratio, $\rho_o/\rho_m$
$a$	Available vertical acceleration ( $\text{m s}^{-2}$ )
$g$	Observed environmental acceleration ceiling under full contrast ( $\text{m s}^{-2}$ )
$V$	Volume ( $\text{m}^3$ )
$C$	Participation coefficient of the added-mass family (dimensionless)
$R_{\text{eff}}$	Effective motion-resistance term (object load + participating medium load)
$F_{\text{net}}$	Net density-driven force = $Vg(\rho_o - \rho_m)$
$v_t$	Terminal velocity in a real medium ( $\text{m s}^{-1}$ )
$\beta_T$	Thermal volumetric expansion coefficient ( $\text{K}^{-1}$ )
$\eta$	Dynamic viscosity of the medium ( $\text{Pa}\cdot\text{s}$ )
$C_d, A$	Drag coefficient (dimensionless); projected area ( $\text{m}^2$ )

## 1. Introduction

Bodies in an environment rest, rise, fall, suspend, accelerate, and reach terminal motion in ways that depend on their density relations with their surroundings. Standard teaching distributes

the explanation of these behaviours across several constructs: gravity, buoyancy, weight, drag, and resistance. ValerieX asks whether the same range of observations can be organised under one prior question:

*Can vertical motion be built from density-state disequilibrium alone?*

This paper develops that question into a symmetry-based reorganisation of classical buoyancy and added-mass behaviour. It is fully consistent with the recognised buoyancy-plus-added-mass family of fluid mechanics (Lamb, 1932; Brennen, 1982; Kelvin, 1871) and is not a refutation of Newtonian or relativistic mechanics. The governing equations recover classical results across the C-family. Novelty lies in the structural reorganisation:  $\chi$  as a bounded organising variable, the drive/coupling/resistance separation, the regime classification, and a unified single-law-plus-pathway-condition reading of the principal observables.

The framing adopted throughout this paper is deliberately twofold. The testable contributions — the symmetry derivation of  $\chi$ , the regime classification, and the C-family validation programme — are presented first in each section and stand independently of any ontological commitment. The motion-first interpretive reading — density-state disequilibrium as the underlying motion driver, with classical gravity-plus-buoyancy recovered as an effective description that captures the correct observables in terrestrial conditions — is then stated openly. The two coincide numerically across the regimes tested here precisely because the classical net force term  $Vg(\rho_o - \rho_m)$  is mathematically identical to the ValerieX drive term. The distinction is structural and interpretive: ValerieX derives the bounded relational law from symmetry principles, organises the response under one drive term rather than multiple primitive force terms, and introduces an explicit regime classification based on pathway availability. Future work may identify regimes (e.g. extreme density contrasts, non-terrestrial environments, or supported-regime configurations) where the interpretations diverge measurably; the present scope does not depend on any such divergence.

Before the technical build, the engine itself is stated plainly. ValerieX reads vertical motion as a single process with four roles. A **drive**: density-state disequilibrium between object and surrounding medium, captured by a bounded relational measure  $\chi$ . A **coupling**: geometry, expressed through the participation coefficient  $C$  of the recognised added-mass family, which sets how the drive translates into early-time acceleration. A **resistance**: viscous and inertial drag, which sets later realised motion. A **pathway condition**: whether the surroundings allow the drive to be realised as acceleration, opposed by a support so it appears as tension, or fully blocked so it appears as weight. The remainder of the paper builds these four roles in order and shows that the same density-state organisation accounts for rest, rise, fall, vacuum free fall, weight-response, buoyancy-response, and terminal motion under one law plus medium participation.

Figure 1 summarises the layered motion-engine organisation used throughout the framework.

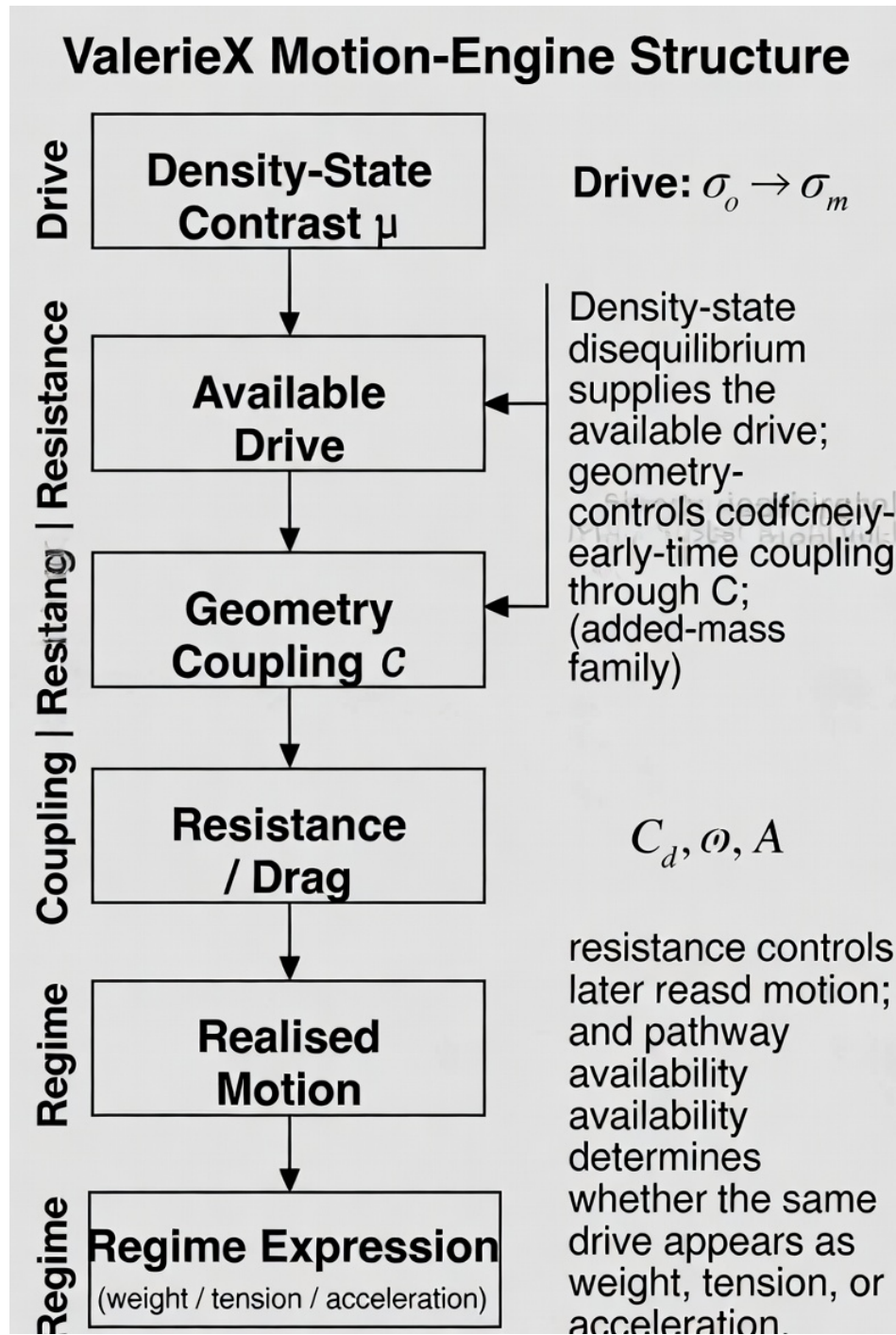


Figure 1: ValerieX motion-engine structure. Density-state disequilibrium supplies the available drive; geometry controls early-time coupling through the participating-medium-load coefficient  $C$ ; resistance governs realised motion through drag and viscous interaction; and pathway availability determines whether the same underlying drive appears as weight, tension, or acceleration.

The development is anchored in observation throughout. Archimedes (c. 250 BCE) on hydrostatic flotation; Galileo (1638) on the medium-independence of vacuum free fall; Bernoulli (1738) and Euler (1757) on fluid pressure; Stokes (1851) and Reynolds (1883) on viscous and inertial drag; Lamb (1932), Landau and Lifshitz (1959), Batchelor (1967), Schlichting and Gersten (2017), and White (2011) on continuum-mechanical closure; Brennen (1982) and McKee and Czarnecki (2019) on added-mass / participating-medium-load; the NIST CODATA reference for  $g$ ; Apollo 15

(Scott, 1971) for vacuum free-fall equality; OpenStax, Chladni (1787), Faraday (1831), Helmholtz (1863), Kundt (1866), and Rayleigh (1877) for acoustic phenomena; ACS for thermal density change; and the U.S. Department of Energy for electromagnetic structuring of substance. The paper does not displace these references; it reorganises the relations between the observables they document.

The purpose of ValerieX is not to replace the successful quantitative machinery of classical fluid mechanics, buoyancy theory, or added-mass formulations. Rather, it proposes that these descriptions can be reorganised under a single density-state motion structure with explicit regime classification, bounded contrast symmetry, and experimentally targetable geometry-coupling behaviour. The framework therefore aims to provide an alternative organisational interpretation of already-successful mechanics while also introducing falsifiable discriminator conditions at early time.

The paper is organised as follows. Section 2 sets out the ontological starting point of density-state disequilibrium. Section 3 introduces the bounded contrast variable  $\chi$  and proves its uniqueness. Section 4 derives Valerie’s Law and gives the working mathematics. Section 5 develops the interpretation of  $g$  as the observed environmental ceiling. Section 6 sets out the geometry-aware C-family extension. Section 7 develops the regime classification of realised motion into constrained, supported, and unconstrained regimes. Section 8 sets out the flagship intermediate-density discriminator at  $\rho_o = 2\rho_m$ . Section 9 summarises the experimental protocol. Section 10 records scope and limitations. Section 11 concludes. Appendix A formalises the higher-degree exclusion argument of §3.4. Appendix B states the full transient drag-coupled ODE referenced in §4.3.3.

## 2. Core Principle: Density-State Disequilibrium

### 2.1. Primitive Entities

ValerieX begins with three primitives: an object characterised by density-state  $\rho_o$ ; an environment or medium characterised by density-state  $\rho_m$ ; and an interaction domain in which both coexist. No primitive upward or downward force is introduced at this stage. Motion is treated as relational, in the spirit of Archimedes (c. 250 BCE) and Galileo (1638).

The framework uses substance rather than matter, volume rather than mass as the primary descriptive basis, and density-state as the primary state variable. These choices are operational, not metaphysical: substance is what physically occupies volume and carries density; volume and density are directly measurable for solids, liquids, and gases (Landau and Lifshitz, 1959; White, 2011). The standard formal definition  $\rho = m/V$  is not denied; it is simply not taken as the primary explanatory starting point.

### 2.2. Disequilibrium as the Source of Motion

The foundational statement of ValerieX is direct:

*Vertical motion arises from density-state disequilibrium between substance and its surrounding environment.*

Define  $\Delta\rho = \rho_o - \rho_m$ . The raw difference is unbounded, so the framework requires a bounded relational measure of disequilibrium. That measure is constructed in Section 3.

Equilibrium is defined by  $\rho_o = \rho_m$ . At this condition there is no vertical motion and no directional preference; rest is state equivalence, not the cancellation of opposing causes. Up and down are not taken as primitive: they emerge from contrast. If  $\rho_o > \rho_m$ , motion resolves one way; if  $\rho_o < \rho_m$ , motion resolves the other. These are observable opposite directions of the same process, not two

independent force categories. “Down” within ValerieX is therefore a contextual direction — the local resolution direction of denser substance through a less-dense surrounding environment, set by the local gradient structure of the medium, not by any absolute or cosmological reference frame.

### 2.3. The Density-State Drive

ValerieX names the physical drive expressed through the framework the **density-state drive** — the contrast-driven acceleration tendency that arises from particle-density disequilibrium between object and surrounding medium within an electromagnetic-field-conditioned environment. It is not a second equation pasted onto the law of Section 4; it is the particle-level meaning of that law. Term for term,  $F_{\text{net}} = Vg(\rho_o - \rho_m)$  is mathematically identical to the classical buoyant net (weight minus Archimedes buoyancy). Within ValerieX this single expression is read as one density-state drive rather than as the sum of two primitive force constructs; the same observable is captured in hydrostatic terms by Archimedes (c. 250 BCE) and organised classically through pressure gradient and buoyancy (Bernoulli, 1738; Euler, 1757; Lamb, 1932). ValerieX identifies it directly at the substance level. The term “density-state drive” names the same observable captured classically by the buoyant net; it does not introduce an additional measured force, and any force-balance computation using  $F_{\text{net}}$  is mathematically interchangeable between the two readings.

### 2.4. Electromagnetic Field as Structural Condition

Within ValerieX, the electromagnetic field is treated as the foundational structural condition that makes differentiated substance, stable phase states, and meaningful density contrasts possible at all. At the microscopic scale it binds electrons to nuclei, governs chemical bonding, and determines the phase behaviour that gives ordinary matter its characteristic densities (U.S. Department of Energy, *The Electromagnetic Force*; DOE, *Quantum Mechanics*; Landau and Lifshitz, 1959). At the macroscopic scale this same field structures the terrestrial environment, enabling the formation of distinct density-states  $\rho_o$  and  $\rho_m$  and the cohesion, adhesion, viscosity, elasticity, and pressure-transmission properties of the surrounding medium.

The electromagnetic field is not introduced here as a competing motion force or as the direct cause of vertical acceleration. ValerieX preserves a strict separation of roles: density-state disequilibrium within the field-conditioned environment supplies the motion driver, expressed through Valerie’s Law  $a = g\chi$  and its geometry-aware C-family extension (§4); EM does not appear directly in either expression, does not derive  $g$ , and does not function as the vertical-motion force. Sound and temperature act as environmental modifiers of density-state through  $\rho_m(t)$  and  $\rho(T)$ . This structural distinction is formalised in Axiom 7.

The roles are layered cleanly. EM stabilises atoms and molecules, permits intermolecular forces (cohesion, adhesion, surface tension), enables viscosity and pressure transmission, and provides the contact and pathway constraints that make constrained- and supported-regime configurations possible. Without EM-conditioned structure,  $\rho_o$  and  $\rho_m$  would not meaningfully exist. The vertical drive sits one layer above this EM substrate and is governed by density-state disequilibrium alone.

The electromagnetic field is therefore treated as a foundational material substrate rather than as a competing vertical-motion force.

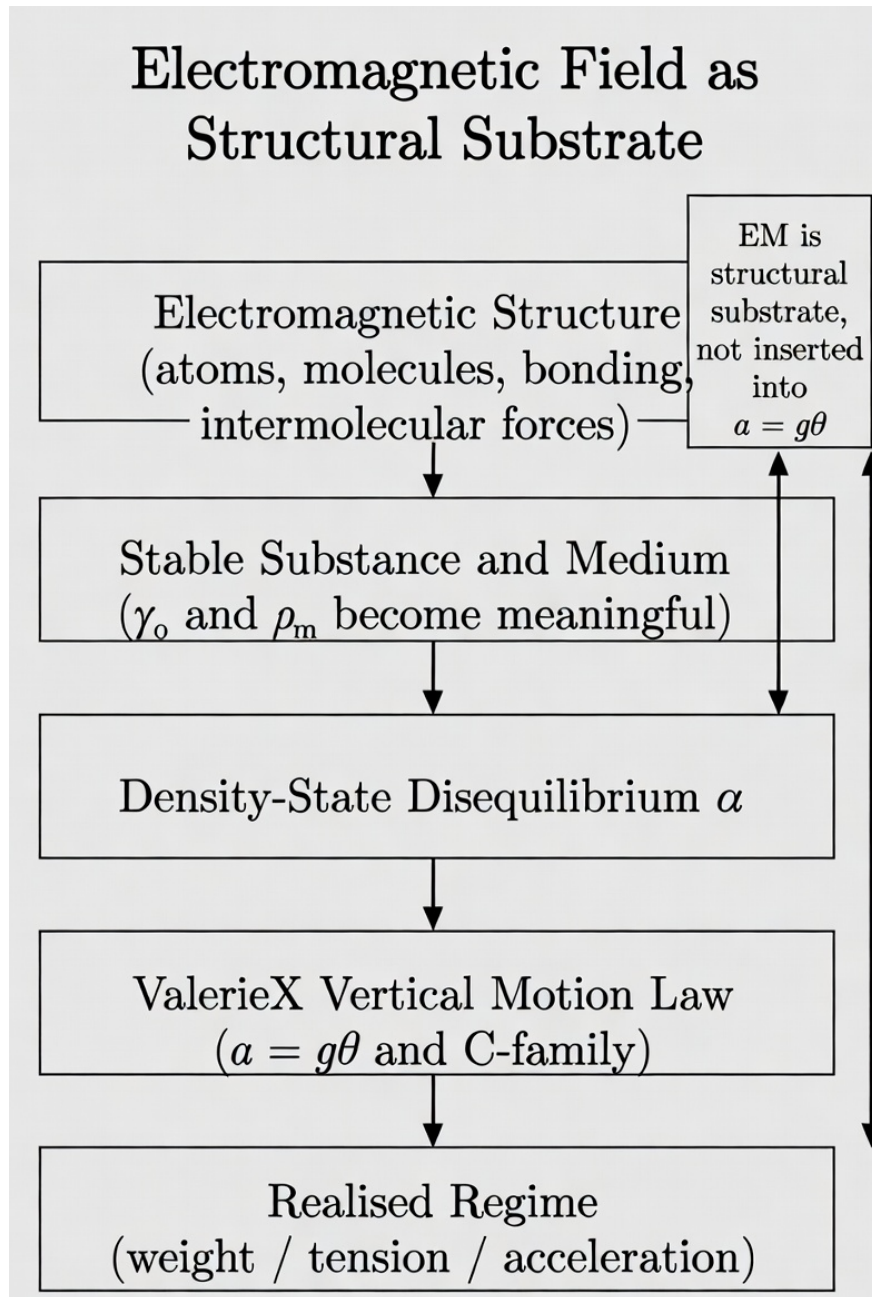


Figure 2: Electromagnetic interactions provide the structural substrate for stable density-states, intermolecular cohesion, viscosity, adhesion, and pathway constraints. ValerieX begins once those density-state systems already exist; electromagnetism is not inserted directly into the governing law.

No claim is made that electromagnetism generates gravity, replaces spacetime descriptions, or directly determines the observed acceleration scale  $g$ ; the electromagnetic field is treated strictly as the structural substrate that permits stable differentiated matter and medium states.

### Vertical motion versus horizontal interaction

Vertical motion in ValerieX is the principal environmental resolution direction of density-state disequilibrium through the surrounding medium. Horizontal motion in an isotropic medium is structurally distinct: it is primarily interaction-driven through contact, propulsion, pressure gradients, momentum transfer, torsion, and direct EM and intermolecular interactions, and is

correctly described by the standard mechanical and EM treatments of those processes. The framework’s claim is restricted to vertical motion under density-state disequilibrium; horizontal interaction-driven motion lies outside its domain by construction.

### Layered EM / ValerieX roles

Layer	EM role	ValerieX role
Substance formation	Stabilises atoms and molecules	Defines measurable $\rho_o$
Medium structure	Permits organised surrounding media	Defines measurable $\rho_m$
Cohesion / adhesion	Produces intermolecular forces and surface tension	Influences pathway conditions
Pressure / viscosity	Enables fluid response and drag	Governs realised resistance
Contact / support	Enables blocked pathways and tensile support	Defines constrained / supported regimes
Vertical motion drive	Not inserted directly	Governed by $\chi$ , Valerie’s Law, and the C-family

### Pedagogical illustration: the dew droplet

A dew droplet on a leaf surface shows the layered structure directly. The droplet exists at all because EM-mediated cohesion holds the water together and EM-mediated adhesion couples it to the leaf surface. These EM-mediated processes set the pathway condition: the droplet is held in the supported regime by adhesion to the surface beneath, even though droplet ( $\rho_o \approx 1000 \text{ kg m}^{-3}$ ) and surrounding air ( $\rho_m \approx 1.225 \text{ kg m}^{-3}$ ) carry the  $\chi \approx +1$  density-state contrast that would otherwise resolve as fall. EM-mediated forces do not generate the  $\chi$ -drive; they hold the realised expression of that drive within a particular regime. When a dew droplet eventually falls — disturbed mechanically, or when adhesion is overcome by accumulated mass — it does so along the same Valerie’s Law branch as any other dense-object-in-air case (§4.3.5).

The dew-droplet example provides an intuitive illustration of how local EM-mediated pathway constraints can coexist with the broader density-state resolution structure.



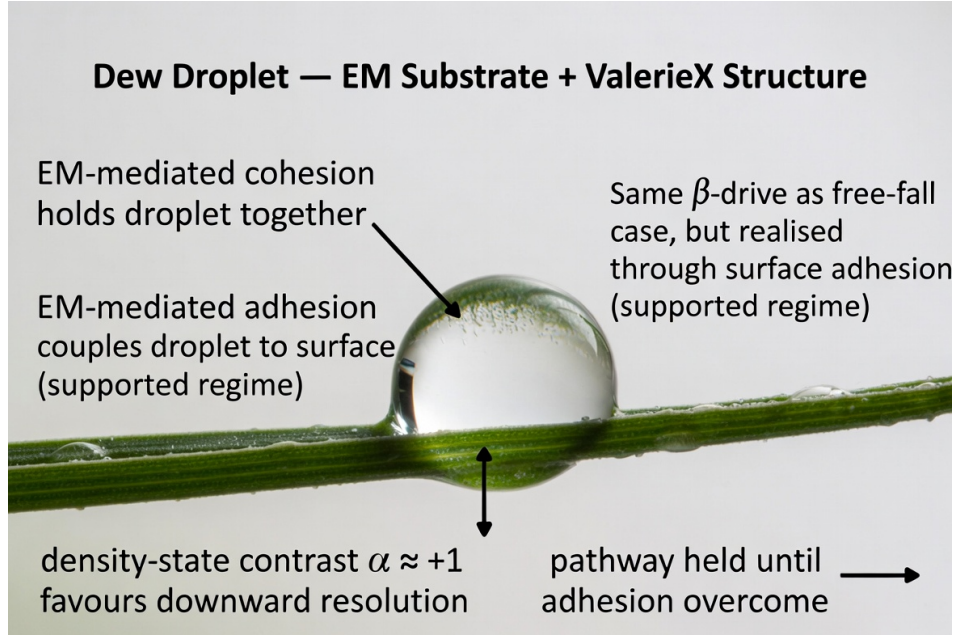


Figure 3: A dew droplet illustrates the coexistence of electromagnetic-mediated adhesion/cohesion and density-state vertical resolution. Surface tension and adhesion temporarily maintain a supported regime while the underlying density-state contrast remains unchanged.

## 2.5. Axioms

Axiom	Statement
1. Relational Motion	Motion is defined only relative to an environment.
2. Density-State Sufficiency	Vertical behaviour is determined by the relation between $\rho_o$ and $\rho_m$ .
3. Disequilibrium Drives Motion	Motion occurs only when $\rho_o \neq \rho_m$ .
4. Bounded Response	Acceleration must remain finite.
5. Symmetry of Contrast	Positive and negative disequilibrium are opposite branches of the same law.
6. Minimal Sufficiency	No structure is introduced unless required by the axioms.
7. Field-Conditioned Differentiation	Differentiated substance and stable density-states are possible because substance exists within a field-conditioned environment.

## 3. The Bounded Contrast Variable $\chi$

### 3.1. Problem Statement

Given the axioms, the task is to determine the relation governing vertical motion in an observable environment. We seek a function  $\chi = f(\rho_o, \rho_m)$  measuring density-state disequilibrium in a bounded, symmetric way. It must satisfy four conditions:

- **Equilibrium:**  $f(\rho_o, \rho_m) = 0$  whenever  $\rho_o = \rho_m$ .
- **Antisymmetry:**  $f(\rho_o, \rho_m) = -f(\rho_m, \rho_o)$ .
- **Scale-neutrality** (homogeneous of degree 0):  $f(\lambda\rho_o, \lambda\rho_m) = f(\rho_o, \rho_m)$  for any  $\lambda > 0$ .

- **Bounded response:**  $|f(\rho_o, \rho_m)| < 1$  for all  $\rho_o, \rho_m > 0$ .

The unique lowest-degree rational form satisfying these four conditions simultaneously, under the standing assumption that  $\chi$  is a rational function of  $(\rho_o, \rho_m)$ , is

$$\chi = \frac{\rho_o - \rho_m}{\rho_o + \rho_m}.$$

The remainder of this section establishes the result in three steps: direct algebraic verification, the lowest-degree minimality argument, and the full characterisation across higher degrees.

This form is also recognised in classical fluid mechanics as the *Atwood number*, which appears naturally in buoyancy-driven flows; ValerieX adopts it as the bounded organising variable of the framework and derives it from the four foundational conditions above.

### 3.2. Algebraic Verification

Let  $\rho_o, \rho_m > 0$ . **Equilibrium:** if  $\rho_o = \rho_m$ , the numerator vanishes and  $\chi = 0$ . **Antisymmetry:**  $\chi(\rho_m, \rho_o) = (\rho_m - \rho_o)/(\rho_m + \rho_o) = -\chi(\rho_o, \rho_m)$ . **Scale-neutrality:**  $\chi(\lambda\rho_o, \lambda\rho_m) = \lambda(\rho_o - \rho_m)/[\lambda(\rho_o + \rho_m)] = \chi(\rho_o, \rho_m)$ . **Boundedness:** by the strict triangle inequality  $|\rho_o - \rho_m| < \rho_o + \rho_m$ , so  $|\chi| < 1$ , with equality approached only in the singular vacuum limits  $\rho_m \rightarrow 0$  ( $\chi \rightarrow +1$ ) and  $\rho_o \rightarrow 0$  ( $\chi \rightarrow -1$ ). All four conditions are satisfied exactly.

### 3.3. Minimality at Lowest Degree

**Step 1.** Scale-neutrality forces a homogeneous-of-degree-0 ratio. Any rational function representing  $\chi$  can be written as  $P(\rho_o, \rho_m)/Q(\rho_o, \rho_m)$ , where  $P$  and  $Q$  are homogeneous polynomials of equal degree  $d$  (otherwise the ratio scales as a non-zero power of  $\lambda$ ).

**Step 2.** Antisymmetry forces parities:  $P$  must be odd under the swap ( $P(\rho_m, \rho_o) = -P(\rho_o, \rho_m)$ ) and  $Q$  even ( $Q(\rho_m, \rho_o) = Q(\rho_o, \rho_m)$ ).

**Step 3.** At lowest degree  $d = 1$ : the only odd linear form (up to scaling) is  $a(\rho_o - \rho_m)$ ; the only even linear form is  $b(\rho_o + \rho_m)$ . Therefore the most general lowest-degree solution to the first three conditions is  $f = k(\rho_o - \rho_m)/(\rho_o + \rho_m)$ , with  $k = a/b \neq 0$ .

**Step 4.** Boundedness fixes  $|k| \leq 1$ , and equality is achieved at the vacuum limits for  $k = \pm 1$ ; the conventional positive sign under positive disequilibrium fixes  $k = +1$ .

The unique lowest-degree rational function satisfying all four conditions is therefore  $\chi = (\rho_o - \rho_m)/(\rho_o + \rho_m)$ .

### 3.4. Higher-Degree Characterisation

It is natural to ask whether higher-degree rational functions can also satisfy the four conditions. They can — but every such solution factors through  $\chi$  multiplied by an even, scale-neutral correction.

By Steps 1–2 above, any solution can be written as  $P/Q$  with  $P$  odd and  $Q$  even of equal degree  $d$ . Because  $P$  is odd and vanishes on the diagonal  $\rho_o = \rho_m$ , it admits the unique factorisation  $P = (\rho_o - \rho_m) \cdot E_1$ , where  $E_1$  is homogeneous of degree  $d - 1$  and even under the swap. The denominator  $Q$  is already even and homogeneous of degree  $d$ . Substituting,

$$f = \chi \cdot \frac{(\rho_o + \rho_m) \cdot E_1}{Q} = \chi \cdot R,$$

where  $R$  is even and scale-neutral. This is the **General Theorem**: every rational solution of the four conditions has the form  $f = \chi \cdot R$  for some even, scale-neutral rational  $R$ . At  $d = 1$ ,

$R$  reduces to a constant fixed by boundedness, and the basic  $\chi$  is recovered. At higher  $d$ , non-trivial  $R$  produces solutions such as  $\chi^3 = \chi \cdot \chi^2$  (with  $R = \chi^2$ ) and other odd-power or composite combinations. These exist algebraically but introduce structure not required by the axioms. By Axiom 6 (minimal sufficiency), ValerieX selects the lowest-degree form: the unadorned  $\chi$ . The formal characterisation of these higher-degree families and the empirical content of the minimal-sufficiency selection are developed in Appendix A.

### 3.5. Properties of $\chi$

For positive density-states,  $-1 < \chi < 1$ . Special cases:  $\chi = 0$  if  $\rho_o = \rho_m$ ;  $\chi \rightarrow +1$  if  $\rho_o \gg \rho_m$ ;  $\chi \rightarrow -1$  if  $\rho_o \ll \rho_m$ . The variable encodes both direction and degree of disequilibrium in one bounded number.

The boundedness structure of the density-state variable is shown in Figure 4.

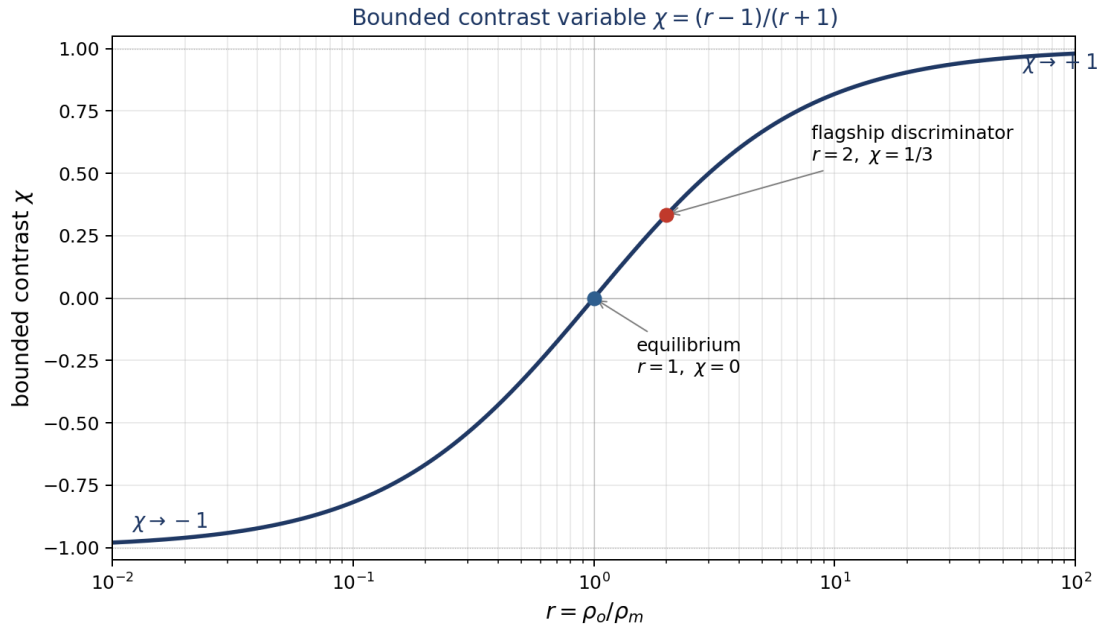


Figure 4: The bounded contrast variable  $\chi = (r - 1)/(r + 1)$ , with  $r = \rho_o/\rho_m$ , maps all positive density ratios into the bounded interval  $-1 < \chi < 1$ . Equilibrium occurs at  $r = 1$  ( $\chi = 0$ ); the flagship discriminator lies at  $r = 2$  ( $\chi = 1/3$ ); and the saturation limits approach  $\chi \rightarrow \pm 1$  in the singular vacuum cases. Analytical curve.

## 4. Valerie's Law: $a = g\chi$

### 4.1. Derivation

By Axiom 3, motion follows disequilibrium. By Axiom 4, motion remains finite. By Axiom 5, opposite contrasts are opposite branches of the same law. The simplest governing relation is linear proportionality between available vertical acceleration and bounded contrast:  $a \propto \chi$ . Introducing the observed environmental scale  $g$  gives **Valerie's Law**:

$$a = g \cdot \frac{\rho_o - \rho_m}{\rho_o + \rho_m} = g\chi.$$

This is the governing law of available vertical motion within ValerieX. It is parameter-free, bounded, antisymmetric, scale-neutral, and continuous. The framework distinguishes *available*

*motion* (set by  $\chi$ ) from *realised motion* (set by environmental constraint); Section 7 develops that distinction through the regime classification.

## 4.2. Independent Derivation from Participating Medium Load

Valerie’s Law also arises from a direct dynamics argument when the effective inertia of the object–environment system is written correctly. The net density-driven force on an object of volume  $V$  is

$$F_{\text{net}} = Vg(\rho_o - \rho_m).$$

In classical terminology, the medium’s inertial participation is described as added mass or virtual mass. ValerieX retains the observable effect but reframes its meaning: it is **participating medium load**, the measurable extent to which surrounding substance must be co-disturbed when disequilibrium resolves (McKee and Czarnecki, 2019; Lamb, 1932). The effective motion-resistance term is

$$R_{\text{eff}} = (\rho_o + C\rho_m)V,$$

where  $C$  is the participation coefficient. The available acceleration is

$$a = \frac{F_{\text{net}}}{R_{\text{eff}}} = g \cdot \frac{\rho_o - \rho_m}{\rho_o + C\rho_m}.$$

Brennen (1982) tabulates classical potential-flow added-mass coefficients: 0.5 for a sphere and 1.0 for a circular cylinder moving perpendicular to its axis. Valerie’s bounded form is recovered exactly at  $C = 1$ : the participating-medium-load coefficient for a circular cylinder moving perpendicular to its axis in inviscid potential flow. The bounded form is therefore not a free ansatz; it is an exact branch of a recognised geometry-dependent family. Interpretively, what classical fluid mechanics calls “mass” in this context is read in ValerieX as participation of the medium in realised motion, not as a foundational cause. This independent mechanistic recovery of the  $C = 1$  branch corresponds to the form fixed in §3 by the four foundational conditions: the symmetry argument and the participating-medium-load argument converge on the same bounded relation.

## 4.3. Working Formulas

### 4.3.1. Core Law and General Form

Bounded core law:

$$a = g \cdot \frac{\rho_o - \rho_m}{\rho_o + \rho_m} = g\chi.$$

Geometry-aware general law:

$$a = g \cdot \frac{\rho_o - \rho_m}{\rho_o + C\rho_m}.$$

Net force, effective resistance, and acceleration:

$$F_{\text{net}} = Vg(\rho_o - \rho_m), \quad R_{\text{eff}} = (\rho_o + C\rho_m)V, \quad a = \frac{F_{\text{net}}}{R_{\text{eff}}}.$$

### 4.3.2. Limiting Regimes

Regime	Condition	Consequence
Equilibrium	$\rho_o = \rho_m$	$\chi = 0, a = 0$ (rest)
Positive disequilibrium	$\rho_o > \rho_m$	$\chi > 0, a > 0$ (denser falls)
Negative disequilibrium	$\rho_o < \rho_m$	$\chi < 0, a < 0$ (lighter rises)
Full positive saturation	$\rho_o \gg \rho_m$	$\chi \rightarrow +1, a \rightarrow +g$ (vacuum-limit fall)
Full negative saturation	$\rho_o \ll \rho_m$	$\chi \rightarrow -1, a \rightarrow -g$ (max-contrast rise)
Near-equilibrium (linear)	$\rho_o = \rho_m + \varepsilon$	$\chi \approx \varepsilon/(2\rho_m), a \approx g\varepsilon/(2\rho_m)$
Antisymmetry swap	$o \leftrightarrow m$	$a(\rho_o, \rho_m) = -a(\rho_m, \rho_o)$

### 4.3.3. Realised Motion and Terminal Velocity

Valerie’s Law gives *available* acceleration. Realised motion is the constrained expression of available motion, mediated by drag in real media. For a low-Reynolds sphere (Stokes, 1851):

$$v_t = \frac{F_{\text{net}}}{6\pi\eta r}.$$

For a general bluff-body regime:

$$v_t = \sqrt{\frac{2 \cdot |\Delta\rho| \cdot g \cdot V}{C_d \cdot \rho_m \cdot A}}.$$

Both are dissipative completions of the picture: density-state disequilibrium sets the drive; the medium sets the constraint; terminal velocity is the realised steady state. These results compose directly with Valerie’s Law without changing its foundation (Stokes, 1851; Reynolds, 1883; Batchelor, 1967; Schlichting and Gersten, 2017; White, 2011). The full transient ODE that interpolates between the early-time C-family acceleration and the drag-limited terminal velocity is given in V3 §8.3, V4 §11, and Appendix B; all three reduce identically to the C-family acceleration at  $v = 0$ .

### 4.3.4. Temperature, Pressure, and Sound as Density-State Modulators

For substances with thermal expansion coefficient  $\beta_T$ ,  $\rho(T) = \rho_0/[1 + \beta_T(T - T_0)]$ ; for gaseous media,  $\rho = pM/(RT)$ . Both relations enter Valerie’s Law directly through  $\rho_m$  (and through  $\rho_o$  where the object contains a compressible substance). Heating reduces  $\rho$ ; cooling raises it; pressure modifies trapped-gas density via Boyle’s Law (Boyle, 1662). These chains govern hot-air balloon rise, convection cells, lava-lamp motion, and Cartesian-diver behaviour (ACS, *Temperature Affects Density*). Sound enters Valerie’s Law as a time-varying  $\rho_m$ , with the pressure wave perturbing the local medium density around its baseline. Resonance occurs where a structure’s natural mode matches the forcing frequency (OpenStax; Rayleigh, 1877). Acoustic levitation and Chladni patterns (Chladni, 1787; Faraday, 1831; Kundt, 1866) are consequences: particles collect at pressure nodes where the local time-averaged contrast is minimal.

### 4.3.5. Worked Examples

Scenario	$\rho_o$	$\rho_m$	$\chi$	$a = g\chi$ (m/s <sup>2</sup> )	Direction
Lead ball in air	11340	1.225	+0.99978	+9.805	falls
Volleyball in air	80	1.225	+0.9699	+9.511	falls
Iron anvil in mercury	7870	13534	−0.2647	−2.596	floats high
Ice in water	917	1000	−0.0433	−0.425	floats low
Volleyball in water	80	1000	−0.8519	−8.353	rises fast
Helium balloon in air	0.179	1.225	−0.7451	−7.305	rises
Hot-air balloon (~100°C)	0.95	1.225	−0.1264	−1.239	rises gently
Air bubble in water	1.225	1000	−0.99756	−9.783	rises maximally
Rock in water	2700	1000	+0.4595	+4.505	sinks
Shuttlecock in air	~100	1.225	+0.9758	+9.568	falls; $v_t \approx 6.80 \text{ m s}^{-1}$
Vacuum (ideal)	any > 0	0	+1.0000	+9.807	universal fall

All densities in kg/m<sup>3</sup>. All cases are described by the same bounded relation  $a = g\chi$ . Every example sits somewhere on the same curve.

### 4.3.6. High-Drag Geometries: The Shuttlecock Example

A badminton shuttlecock provides a vivid, everyday illustration of the same density-state drive operating under strong resistance. The shuttlecock’s effective bulk density (typically ~ 80–120 kg m<sup>−3</sup> against air at 1.225 kg m<sup>−3</sup>) gives  $\chi \rightarrow +1$ , so Valerie’s Law specifies an available acceleration  $a \rightarrow g$ . The realised motion, however, is dominated almost immediately by the bluff-body drag closure of §4.3.3: with  $C_d \approx 0.65$  for the standard skirt geometry, the bluff-body terminal-velocity formula gives  $v_t \approx 6.80 \text{ m s}^{-1}$ , and 99% of terminal velocity is reached in 1.84 s after a fall of 9.2 m (Peastrel, Lynch and Armenti, 1980).

The shuttlecock is therefore the high-drag complement to the dense-object-in-air rows of §4.3.5. Both share  $\chi \rightarrow +1$ ; they differ entirely in how rapidly drag closes the gap between available and realised motion. The cork-forward orientation stability emerges from the internal mass distribution and skirt geometry, illustrating how geometry controls the realised pathway even when the underlying drive is near saturation (§6.3). Feather and synthetic versions provide a clean home experiment: holding  $\chi$  fixed and varying  $C_d$  across the two skirt constructions tests the resistance branch of the drive–coupling–resistance separation directly. A phone high-speed video from a stairwell ( $\geq 5 \text{ m}$  fall) resolves both the rapid approach to terminal velocity and the orientation self-stabilisation, with no tank or precision release required.

## 4.4. Classical Results Recovered

ValerieX is mathematically identical to the buoyancy-plus-added-mass family of classical fluid mechanics across the full range of in-scope phenomena. The table below makes the equivalence explicit: each standard textbook result emerges as a specific expression of the density-state drive  $Vg(\rho_o - \rho_m)$  under a specific regime and pathway condition.

Classical result	Standard form	ValerieX form	Equivalence
Archimedean buoyancy (Archimedes, c. 250 BCE)	$F_b = \rho_m g V$	$F_{\text{net}} = Vg(\rho_o - \rho_m); \chi = 0$ at flotation depth	Identical net force; ValerieX reads it as one drive rather than weight minus buoyancy
Newtonian weight (terrestrial, in air)	$W = mg$	$F_{\text{net}} \approx V\rho_o g$ (since $\rho_m \ll \rho_o$ ); $a \rightarrow g$ as $\chi \rightarrow 1$	Identical to within the air-buoyancy correction ( $\sim 10^{-4}$ for solids)
Vacuum free fall (Galileo 1638; Apollo 15)	$a = g$	$a = g\chi \rightarrow g$ as $\rho_m \rightarrow 0$ , every $C$ , every $C_d$	Identical; geometry, viscosity, drag collapse out simultaneously
Atwood number (classical fluid mechanics)	$A = (\rho_1 - \rho_2)/(\rho_1 + \rho_2)$	$\chi = (\rho_o - \rho_m)/(\rho_o + \rho_m)$	Mathematically identical; ValerieX derives it from the four foundational conditions of §3
Added-mass coefficient, sphere (Lamb 1932; Brennen 1982)	$k = 0.5$	$C = 0.5$ branch of $a = g(\rho_o - \rho_m)/(\rho_o + C\rho_m)$	Identical; recovers McKee and Czarnecki (2019)
Added-mass coefficient, cylinder $\perp$ axis (Kelvin 1871; Lamb 1932)	$k = 1.0$	$C = 1$ branch; recovers $a = g\chi$ exactly	Identical; the bounded branch on which label-exchange antisymmetry holds for the full law
Stokes terminal velocity, low Re (Stokes 1851)	$v_t = 2(\rho_o - \rho_m)gr^2/(9\eta)$	$v_t = F_{\text{net}}/(6\pi\eta r)$ , $F_{\text{net}} = Vg(\rho_o - \rho_m)$	Identical
Bluff-body terminal velocity, high Re	$v_t = \sqrt{2 \Delta\rho gV/(C_d\rho_m A)}$	Same expression with $F_{\text{net}} = Vg(\rho_o - \rho_m)$ carried through	Identical
Hydrostatic equilibrium in stratified medium	$\rho_o = \rho_{\text{local}}$ at suspension layer	$\chi = 0$ at suspension layer	Identical

The point of this table is structural rather than computational: every standard result is a specific expression of the same density-state drive under a specific regime and pathway condition. ValerieX is not in competition with any of these results. Its contribution is to organise their differences as differences of regime, coupling, and pathway availability rather than as differences of physical primitive.

## 5. Interpretation of $g$ as the Observed Environmental Ceiling

Within ValerieX,  $g$  is taken as a primitive observed environmental quantity rather than as a derived one. It is the maximum realised vertical particle acceleration available in the local environment under full contrast. NIST gives the standard acceleration of gravity as exactly  $9.80665 \text{ m s}^{-2}$  (NIST CODATA). ValerieX treats that near-surface terrestrial value as the observed ceiling. Classical mechanics derives the local value of  $g$  from Newtonian gravitation as  $g = GM_E/r^2$  together with Earth's mass, radius, and rotational/oblateness corrections, and predicts its variation with altitude, latitude, and planetary body. ValerieX makes no equivalent derivation; this represents a scope boundary relative to the classical gravitational derivation and is stated as such. Within the present scope of terrestrial vertical motion,  $g$  enters the framework as an observed environmental ceiling and its near-surface value is taken from measurement.

The vacuum case is where the ceiling is most cleanly revealed: as  $\rho_m \rightarrow 0$ , every positive-density object enters the same maximum contrast condition, so all bodies share the same realised acceleration. Substituting  $\rho_m \rightarrow 0$  into Valerie's Law gives  $a = g$  for any positive  $\rho_o$ . In the vacuum limit, the ratio  $\rho_o/\rho_m \rightarrow \infty$ , so all positive-density objects are infinitely denser than the surrounding medium in the limiting ratio sense and therefore occupy the same maximum-contrast state with  $\chi \rightarrow 1$ . This does not imply infinite object density. Universal free-fall equality follows directly. This is the observable demonstrated on the lunar surface during Apollo 15 (Scott, 1971), in line with Galileo (1638). More generally, in the vacuum limit the participating medium load  $C\rho_m$  vanishes for any value of  $C$ ; the geometry-aware general law collapses to  $a = g$  for every C-branch simultaneously, and the medium's viscous resistance also vanishes. Geometry, coupling, and drag have no effect on realised acceleration in this limit.

### 5.1. $g$ as a Pathway-Availability Ceiling

Within ValerieX, the terrestrial acceleration scale  $g = 9.80665 \text{ m s}^{-2}$  (NIST CODATA) is interpreted as the local environmental ceiling of realised vertical acceleration. This value is not treated as the cause of motion itself, but as the maximum realised acceleration permitted when pathway availability is effectively complete. When the downward pathway is fully available, density-state disequilibrium is expressed directly as motion, approaching this environmental ceiling. When pathway availability is reduced or blocked, the same underlying motion tendency is instead expressed as constrained interaction (weight) or balanced by the surrounding environment. This pathway-availability reading provides the link between the scalar law  $a = g\chi$  and the regime classification developed in Section 7.

The framework makes no claim to derive  $g$  from first principles, and it does not propose a mechanism for the terrestrial acceleration ceiling beyond its status as a measured environmental quantity. Any extension of ValerieX into non-terrestrial environments would require independent measurement of the local ceiling and is outside the scope of the present formulation.

### 5.2. Vacuum Collapse of Geometry and Resistance

The vacuum limit gives a direct structural reading of the motion engine. Substituting  $\rho_m \rightarrow 0$  into the geometry-aware general law,

$$a \rightarrow g \cdot \frac{\rho_o - 0}{\rho_o + C \cdot 0} = g,$$

for every positive  $\rho_o$  and every finite  $C$ . The participating medium load  $C\rho_m$  vanishes, and the medium's viscous resistance vanishes simultaneously. Geometry, coupling, viscosity, drag, and medium participation all collapse out together.



ValerieX reads vacuum universality directly as the saturation limit of density-state contrast. All positive-density objects occupy the same maximum contrast state relative to a zero-density medium ( $\chi \rightarrow +1$ ), so all bodies share the same realised acceleration. The Apollo 15 hammer-and-feather demonstration (Scott, 1971) is the visible signature of this collapse. This is a structural derivation of why geometry, viscosity, and density differences cease to matter once the medium term vanishes; it is not a first-principles derivation of terrestrial  $g$ , which remains a measured environmental quantity throughout the framework.

## 6. The C-Family: Geometry-Aware Extension

### 6.1. The C-Family of Acceleration Laws

In real media the surrounding substance does not participate uniformly. The realised acceleration depends on the geometric manner in which the object disturbs and is dynamically coupled to the medium. The geometry-aware general law is therefore

$$a = g \cdot \frac{\rho_o - \rho_m}{\rho_o + C\rho_m},$$

with the following recognised values (Brennen, 1982; Lamb, 1932; Kelvin, 1871):

- $C \rightarrow 0$ : negligible medium participation (vacuum limit or strict object-normalised form);
- $C = 0.5$ : spherical objects in inviscid potential flow;
- $C = 1$ : cylinders moving perpendicular to their axes (the ValerieX bounded branch).

The geometry-coupling coefficient  $C$  is not introduced as a free phenomenological fitting term, but as a compact motion-engine representation of the participating-medium-load behaviour already studied within classical added-mass theory for accelerating bodies in fluids.

Valerie’s Law is recovered identically at  $C = 1$ .  $C$  is not a universal constant: in real systems it is set by geometry and medium interaction, with the classical values recovered within the same framework. The  $C = 0.5$  sphere branch and  $C \rightarrow 0$  strict object-normalised branch retain their classical scope and provide the basis for the shape-controlled measurements proposed in Section 9.

Figure 5 shows how geometry-dependent participating-medium-load modifies the realised early-time acceleration despite identical density ratios.

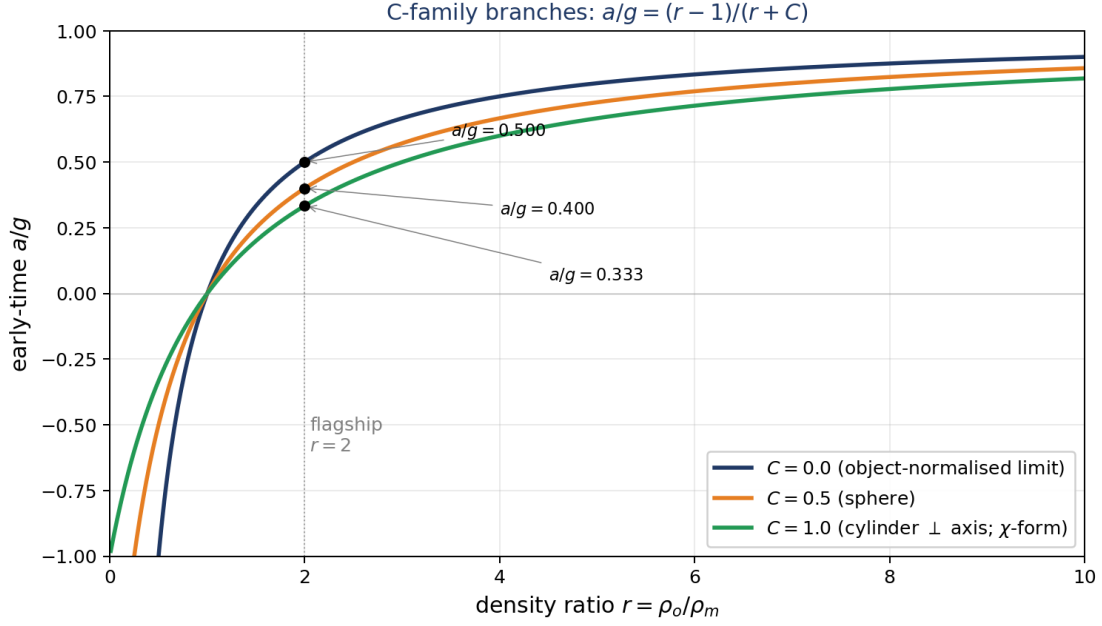


Figure 5: Geometry-dependent early-time acceleration branches predicted by the C-family relation  $a/g = (r - 1)/(r + C)$ . The branches correspond to  $C = 0$  (strict object-normalised limit, no medium participation),  $C = 0.5$  (sphere in inviscid potential flow), and  $C = 1$  (cylinder perpendicular to axis; the ValerieX bounded branch). All three branches converge at saturation ( $r \rightarrow \infty$ ); they diverge progressively as  $r$  decreases. At the flagship discriminator  $r = 2$  the predicted separations are  $a/g = 0.500, 0.400$ , and  $0.333$  respectively — experimentally accessible margins. Analytical curves.

## 6.2. The $C = 1$ Branch within the Family

The four foundational conditions of §3 apply to the acceleration law as a whole, not only to the bounded contrast variable  $\chi$ . Equilibrium and scale-neutrality are satisfied throughout the family. Antisymmetry under exchange of density labels  $\rho_o \leftrightarrow \rho_m$ , however, places a non-trivial constraint on the denominator. Direct exchange of densities gives

$$a(\rho_o, \rho_m) = -a(\rho_m, \rho_o) \Leftrightarrow \rho_o + C\rho_m = \rho_m + C\rho_o,$$

which simplifies to  $(1 - C)(\rho_o - \rho_m) = 0$  and so requires  $C = 1$  for all  $\rho_o \neq \rho_m$ . Boundedness then follows automatically: at  $C = 1$  the strict triangle inequality  $|\rho_o - \rho_m| < \rho_o + \rho_m$  gives  $|a/g| < 1$ , with equality approached only in the singular vacuum limits.

This is a label-exchange algebraic property of the C-family, not a physical privileging of any particular configuration.  $C = 1$  is the algebraic branch on which label-exchange antisymmetry holds for the full law; in real systems  $C$  remains geometry-dependent across the C-family. The  $C = 1$  branch is the bounded member of the family on which Valerie’s Law is recovered, and it coincides classically with the cylinder  $\perp$  axis added-mass coefficient (Kelvin, 1871; Lamb, 1932; Brennen, 1982). The  $C = 0.5$  sphere branch and  $C \rightarrow 0$  strict object-normalised branch retain their classical scope, and  $C$  in any given configuration is determined by geometry and medium interaction rather than by an algebraic preference.

## 6.3. Geometry as a Discriminator

The geometry-aware extension admits a direct empirical reading. Geometry controls how an object couples to its surrounding medium: it determines how much of the medium is co-disturbed

when motion is realised, and therefore which member of the C-family describes the early-time acceleration. In the vacuum limit ( $\rho_m \rightarrow 0$ ) every C-branch collapses to the same value  $a = g$ , and geometry plays no role; this is the regime in which the Apollo 15 hammer-and-feather demonstration (Scott, 1971) is exact. At finite  $\rho_m$ , the amount of participating medium load depends on shape, orientation, and surface interaction with the surrounding substance (Brennen, 1982; Lamb, 1932).

Within ValerieX, this gives a sharp discriminator: spheres minimise orientation effects and are predicted to track the inviscid-sphere branch ( $C = 0.5$ ); cylinders moving perpendicular to their axes are predicted to track the  $C = 1$  branch. Other geometries (cubes, hemispherical-ended capsules, irregular bodies) introduce orientation-dependent coupling whose realised acceleration sits between these branches and varies with attitude. The shape-controlled measurement programme of Section 9 follows directly from this structure.

*Geometry shapes the realisation of density-state disequilibrium by controlling how the object displaces, disturbs, and couples to the surrounding medium.*

Geometry does not generate motion. Density-state contrast is the engine of motion. Geometry controls how the object couples to the surrounding medium once motion is expressed: at the instant of release, this coupling appears through  $C$ ; as velocity develops, the same coupling composes with the medium's viscous and inertial resistance to produce drag. Depending on shape, orientation, and surface interaction, geometry can either reduce or increase this resistance.

#### 6.4. The Capsule Continuous Discriminator

A central computational result developed in V3 §6 is the prediction for the capsule (hemisphere-ended cylinder) participation coefficient as a function of cylindrical-section aspect ratio  $L/D$ , computed from the closed-form added-mass coefficient for a prolate spheroid in motion perpendicular to its long axis (Lamb, 1932 §126; Brennen, 1982 Table 1). For a prolate spheroid with semi-major axis  $a$  and semi-minor axis  $b$ , motion perpendicular to the long axis gives an added-mass coefficient  $k_\perp = \beta_0/(2 - \beta_0)$ , where  $\beta_0 = 1/e^2 - [(1 - e^2)/(2e^3)] \cdot \ln[(1 + e)/(1 - e)]$  and  $e = \sqrt{1 - (b/a)^2}$  is the spheroid eccentricity. For a capsule of cylindrical-section length  $L$  and end-cap diameter  $D$ , the body is mapped to an equivalent prolate spheroid of aspect ratio  $a/b = (L/D) + 1$ , which matches both limits exactly: at  $L/D = 0$  the capsule is a sphere ( $a/b = 1$ ,  $k_\perp = 0.5$ ); as  $L/D \rightarrow \infty$  the capsule approaches an infinite cylinder ( $a/b \rightarrow \infty$ ,  $k_\perp \rightarrow 1$ ).  $C = k_\perp$  in our notation.

$L/D$	Spheroid $a/b$	Predicted $C$	$a/g$ at $r = 2$	$a$ at $r = 2$ (m s <sup>-2</sup> )
0.0	1.00	0.500	0.4000	3.923
0.5	1.50	0.580	0.3949	3.872
1.0	2.00	0.704	0.3698	3.626
1.5	2.50	0.781	0.3601	3.531
2.0	3.00	0.804	0.3566	3.498
3.0	4.00	0.864	0.3494	3.426
4.0	5.00	0.890	0.3461	3.394
6.0	7.00	0.929	0.3414	3.348
8.0	9.00	0.954	0.3386	3.320

The curve passes exactly through the sphere limit  $C = 0.5$  at  $L/D = 0$  and approaches the cylinder  $\perp$  axis limit  $C = 1$  monotonically as  $L/D$  grows. This converts the capsule shape-controlled experiment from a binary sphere-vs-cylinder discriminator into a continuous-parameter falsification test: any monotonic  $L/D$  trend in measured early-time acceleration that does not track this curve would directly challenge the prolate-spheroid mapping or the C-family struc-

ture. The mapping  $a/b = (L/D) + 1$  is a first-order approximation; CFD or boundary-element calculation can produce a more accurate curve if needed. The ordering predicted here —  $a_{\text{sphere}}(r) > a_{\text{capsule}}(r) > a_{\text{cylinder}}(r)$  at fixed  $r > 1$ , monotonic in  $L/D$  — is the structural prediction of the framework and does not depend sensitively on the spheroid mapping.

The capsule curve converts the sphere–cylinder comparison into a continuous falsification target rather than a binary geometry test (Figure 6).

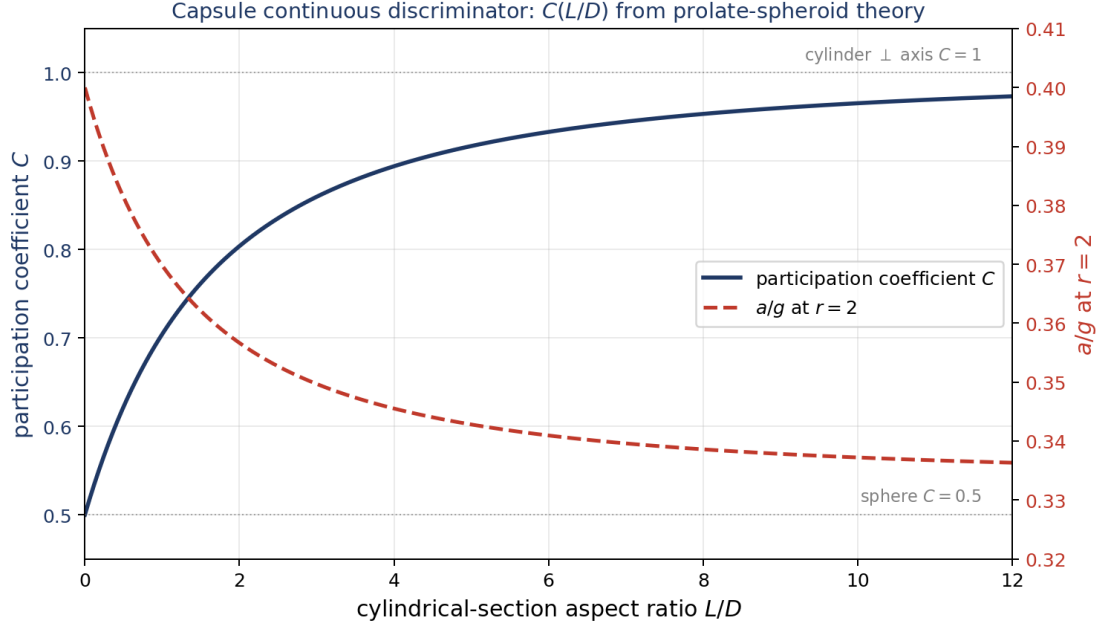


Figure 6: Continuous geometry discriminator derived from prolate-spheroid added-mass theory. Increasing cylindrical-section aspect ratio  $L/D$  shifts the participating-medium-load coefficient  $C$  monotonically from the sphere limit ( $C = 0.5$  at  $L/D = 0$ ) toward the cylinder  $\perp$  axis limit ( $C \rightarrow 1$  as  $L/D \rightarrow \infty$ ). The right-hand axis shows the corresponding predicted  $a/g$  at the flagship discriminator  $r = 2$ , decreasing from 0.400 to 0.333 across the same range. Analytical curve from the closed-form prolate-spheroid mapping  $a/b = (L/D) + 1$  (Lamb 1932 §126; Brennen 1982 Table 1).

## 7. Regimes: Constrained, Supported, Unconstrained

### 7.1. Why Regime Classification Is Required

ValerieX distinguishes *available* motion (set by  $\chi$ ) from *realised* motion (set by environmental constraint). That alone forces classification. Valerie’s Law gives one number — available acceleration  $a = g\chi$  — for any pair  $(\rho_o, \rho_m)$ . But the realised behaviour at the same  $(\rho_o, \rho_m)$  is not one number. A lead ball at rest on a table, hanging from a wire, and in free fall all share the same  $\chi$ . They differ in how the available motion is expressed. That difference is not described by  $\chi$ ; it is described by the environment’s relationship to the downward pathway.

A regime is determined by **pathway availability**. Whether downward motion is blocked, held, or free determines how the same density-state drive is expressed. The regime is read directly from the configuration. The classification adds no new physical content to the framework; it names and organises the realised-motion structure that the available/realised distinction already establishes.

## 7.2. The Three Regimes

**Constrained Motion** The downward pathway is physically blocked by a rigid surface beneath the object. Motion is prevented. Density-state disequilibrium cannot resolve through displacement and is instead expressed as a sustained, measurable contact interaction at the point of support. **Weight is the realised expression of constrained vertical motion under blocked pathway availability.** The constrained regime is the regime in which weight is realised. A weighing scale is a constrained-regime instrument; its reading is the force-response at the point of support produced by the environment's blocking of the otherwise-available resolution of  $\chi$ . Operational signature: a rigid surface is present beneath the object, the object is in contact with it, and the surface prevents further vertical resolution. All surface-supported rest states fall in this regime.

**Supported Motion** The object is held from above by a string, wire, cable, fibre, or other tension element, while the downward pathway beneath the object remains physically open. No rigid surface blocks descent. Motion is not realised, but the non-realisation is accomplished by tensile support from above, not by obstruction from below. This regime is structurally distinct from the constrained regime even though both share the observation of zero realised motion. In the constrained regime motion is *blocked*; in the supported regime motion is *held*. ValerieX identifies the measured tension in the supporting element as the transmitted density-state drive: the unresolved drive of non-realised motion, transmitted through the supporting element rather than through a blocking surface. Operational signature: a tension element bears the object from above, and there is visible clearance — air, fluid, or vacuum — beneath it. A chandelier on a hook, a plumb bob, a mass on a spring scale, and a Cavendish-balance test mass all operate in this regime.

**Unconstrained Motion** The downward pathway is fully open and no external element holds the object. Density-state disequilibrium resolves through motion itself. Available motion is realised to the extent that the medium permits; in vacuum, available and realised motion coincide and the object accelerates at the environmental ceiling  $g$ . This is the regime in which Valerie's Law operates in its most directly expressive form. No interpretive layer sits between the density-state drive and the observed motion. The Apollo 15 hammer-and-feather demonstration (Scott, 1971) is the canonical visual anchor:  $\rho_m \rightarrow 0$  collapses every positive-density object onto the same  $\chi \rightarrow +1$  and the resulting realised acceleration is  $g$  for all. The unconstrained regime also covers everyday cases in air where drag partially constrains the pathway. Valerie's Law still supplies the available drive, and the realised motion is its expression under the available pathway conditions. Terminal velocity is the realised steady-state outcome of progressive pathway constraint; the regime remains unconstrained in the structural sense that no blocking surface or tensile support is present.

Figure 7 illustrates how identical density-state drive can manifest differently depending on environmental pathway conditions.

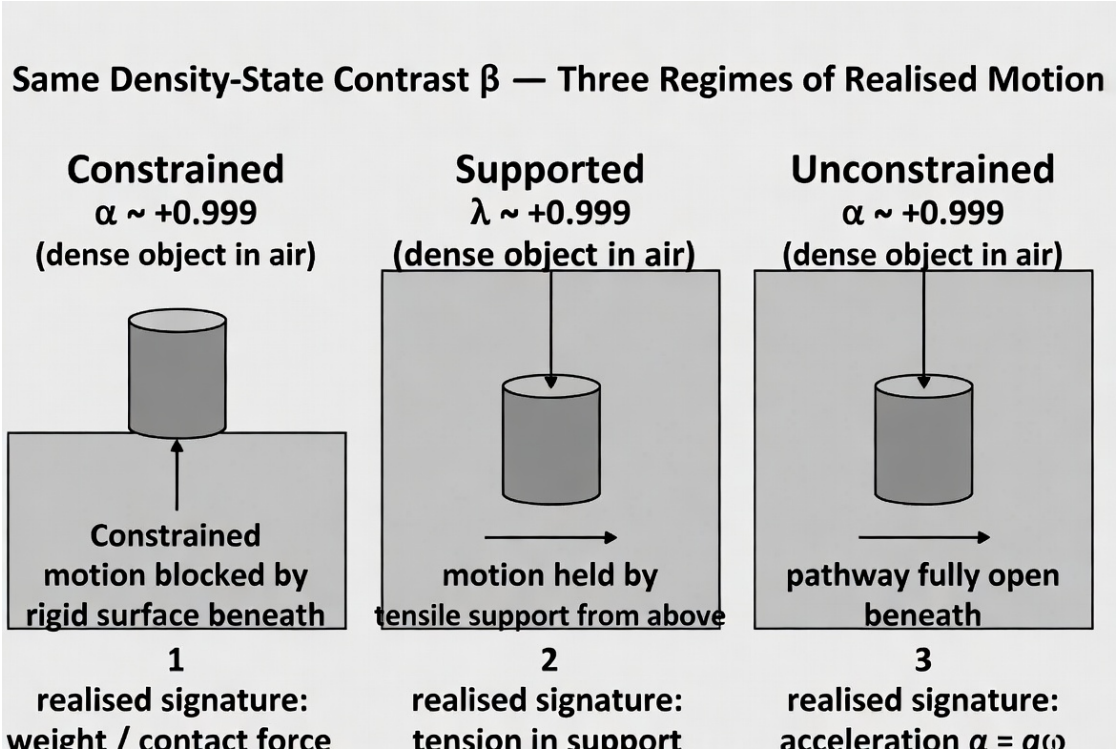


Figure 7: The same density-state contrast may appear as weight/contact force, tensile support, or acceleration depending on pathway availability. The underlying drive remains unchanged; only the realised expression differs.

7.3. The Operational Criterion

The classification of any system is determined by a single observable condition:

*Is the downward pathway physically blocked by a rigid surface beneath the object, held by a tensile element from above, or fully open?*

7.4. Regime Summary

Regime	Pathway condition	Realised outcome	ValerieX reading
Constrained	Blocked by rigid surface	Motion prevented; force at contact	Weight realised
Supported	Held from above; clear beneath	Motion not realised; tension in support	Density-state drive transmitted; weight not realised
Unconstrained	Fully open beneath	Motion realised; $a \rightarrow g\chi$ , bounded by medium	Valerie’s Law expressed directly

7.5. The Same  $\chi$  in Different Regimes

The same  $\chi$  can appear in all three regimes, and the regime — not  $\chi$  alone — determines the measurable signature. The brick-on-table, brick-hung, brick-dropped triplet shares identical  $\chi \approx +0.999$  against air; what differs is how that  $\chi$ -drive is environmentally expressed. The regime classification therefore replaces force-first vocabulary, where the same object is said to experience different forces in different contexts (gravity and buoyancy, gravity and drag, gravity

and normal force, and so on), with a unified reading: the object experiences one density-state drive, and the environment expresses it in one of three regimes. There is no need to multiply forces to match the observations.

Scenario	$\rho_o$	$\rho_m$	$\chi$	Regime
Brick on table, air	$\sim 1800$	1.225	+0.9986	Constrained
Brick hung from string, air	$\sim 1800$	1.225	+0.9986	Supported
Brick dropped in air	$\sim 1800$	1.225	+0.9986	Unconstrained
Iron anvil in mercury	7870	13534	−0.2647	Unconstrained (buoyant)
Volleyball held under water	80	1000	−0.8519	Unconstrained (buoyant)
Air bubble in water	1.225	1000	−0.9976	Unconstrained (buoyant)
Cavendish test mass, air	$\sim 11340$	1.225	+0.99978	Supported
Apollo 15 hammer, lunar vacuum	$\sim 2700$	$\rightarrow 0$	$\rightarrow +1$	Unconstrained (vacuum)
Helium balloon, air	0.179	1.225	−0.7451	Unconstrained (rising)

The first three rows make the point vividly. The same brick has the same  $\chi$  in all three regimes. The signature it leaves in the world — scale reading, string tension, or realised fall — is completely different. The regime is where the difference lives;  $\chi$  is where the drive lives.

## 7.6. Pathway Availability and the Realisation of Weight

Within ValerieX, weight is not treated as a continuously expressed property, but as a realised condition arising from environmental constraint. Weight does not appear or disappear; it is either realised or unrealised depending on pathway availability. The unified statement is direct:

*Density contrast defines the available motion tendency. Pathway availability determines whether that tendency is realised as motion, tension, or weight. Surrounding-environment displacement determines equilibrium.*

Equilibrium under ValerieX is not the absence of disequilibrium but its balanced expression against the surrounding environment. When the local environment fully displaces the downward motion tendency — as for a body suspended in a fluid at the layer where  $\rho_o = \rho_{\text{local}}$  —  $\chi$  vanishes and no realised motion follows. Density-column stratification, Cartesian diver behaviour, and floating bodies in liquids are all recovered as expressions of this principle.

## 7.7. Same Drive, Different Realised Signature

Classical language describes the same object differently depending on context: weight on a table, tension on a string, acceleration in free fall, buoyant response in a fluid. ValerieX claims that the cleaner invariant is the bounded contrast variable  $\chi$ . The same  $\chi$  can appear as a scale reading in the constrained regime, as tension in the supported regime, or as acceleration in the unconstrained regime.

The motion-engine prediction is therefore organisational rather than purely numerical:

*The measured quantity changes because pathway availability changes, not because the density-state drive changes.*

ValerieX accordingly predicts that regime transition experiments should preserve the same un-

derlying density-state drive while changing only the realised channel of expression. A drop-box scale reading going to near zero during free fall (Experiment 3, §9.4) is not interpreted as the disappearance of the drive, but as the removal of the constrained-regime pathway that realises weight. The  $\chi$ -drive itself is invariant under the transition; only the realised channel — surface contact, tensile support, or open-pathway acceleration — changes. This is the framework’s reading of the regime classification of §7.2 and the operational basis on which the regime-transition tests of §9.4 are designed.

## 8. The Flagship Practical Prediction: $r = 2$

### 8.1. The Discrimination Region

All three branches of the C-family converge at full positive saturation ( $r \gg 1$ ) — this is why dense-object-in-air drop tests do not discriminate the family. They diverge progressively as  $r$  decreases. The  $C = 0$  column produces  $|a/g| > 1$  for every case where  $\rho_o < \rho_m$  — an outcome inconsistent with observed bounded buoyant rise once added-mass effects are properly accounted for (McKee and Czarnecki, 2019). Only the  $C = 1$  (ValerieX) branch is bounded throughout. The intermediate-falling regime ( $1 < r \lesssim 5$ ) is the experimentally optimal discrimination region: predictions differ by an experimentally accessible margin while both branches remain physically meaningful and within the dynamic range of accessible apparatus.

System	$\rho_o$	$\rho_m$	$r$	$\chi$	$C=1$	$C=0$	$C=0.5$
Air bubble in water	1.225	1000	$1.23 \times 10^{-3}$	-0.9976	-0.9976	-815.3 ‡	-1.99 ‡
Volleyball in water	80	1000	0.080	-0.8519	-0.8519	-11.5 ‡	-1.59 ‡
Helium balloon in air	0.179	1.225	0.146	-0.7451	-0.7451	-5.84 ‡	-1.32 ‡
Ice in water	917	1000	0.917	-0.0433	-0.0433	-0.0905	-0.0586
Flagship: $\rho_o=2\rho_m$	2000	1000	2.000	+0.3333	+0.3333	+0.5000	+0.4000
Rock in water	2700	1000	2.700	+0.4595	+0.4595	+0.6296	+0.5313
Lead ball in air	11340	1.225	9257	+0.99978	+0.99978	+0.99989	+0.99984

‡ Indicates  $|a/g| > 1$ , i.e. the strict object-normalised or sphere prediction exceeds the vacuum-limit ceiling. These divergent values are systematic outputs of the  $C = 0$  (and  $C = 0.5$ ) formulas whenever  $\rho_o < \rho_m$ , and are the visible signature of the bounded  $C = 1$  branch within the family.

### 8.2. The Flagship Prediction at $\rho_o = 2\rho_m$

At  $r = 2$ , the C-family predictions separate by experimentally accessible margins:

Branch	$C$	$a/g$	$a$ (m s <sup>-2</sup> )
Classical (no added-mass)	0	0.5000	4.903
Sphere (potential flow)	0.5	0.4000	3.923
ValerieX (cylinder $\perp$ axis)	1	0.3333	3.269

The  $C = 0$  vs  $C = 1$  separation is approximately  $0.167g \approx 1.63 \text{ m s}^{-2}$  ( $\sim 33\%$  of  $g$ ). This is an order of magnitude larger than the systematic error of any modern motion-tracking apparatus and is resolvable on commodity high-speed video at  $\geq 240$  fps. The  $C = 0.5$  vs  $C = 1$  (sphere



vs cylinder) separation is approximately  $0.067g \approx 0.65 \text{ m s}^{-2}$  ( $\sim 6.7\%$  of  $g$ ) and requires  $\geq 1000$  fps imaging with sub-millimetre tracking precision: at  $t = 30 \text{ ms}$  after release this corresponds to a position difference of approximately  $0.3 \text{ mm}$  between the two predictions.

### Why the Early-Time Window Matters

Late-time drag closure washes the C-family branches together: every shape settles toward a terminal velocity governed by  $C_d$ , and the geometry-dependent participating-medium-load is no longer separable from the medium-set resistance. The first tens of milliseconds, before drag dominates, are where the C-family lives. At  $r = 2$  in water the  $C = 0$  vs  $C = 1$  acceleration gap is  $\sim 1.6 \text{ m s}^{-2}$  during the first  $30 \text{ ms}$ , then collapses below noise as both branches converge on the same  $v_t$ . Early-time measurement is therefore not an experimental convenience; it is the only window in which the geometry-dependent coupling structure of classical added-mass theory is directly observable in a finite medium. The flagship discriminator is not a fit exercise across the full trajectory but a sharp early-time test of which C-branch the system actually occupies.

The corrected transient evolution under the Section 8 reference conditions is shown in Figure 8.

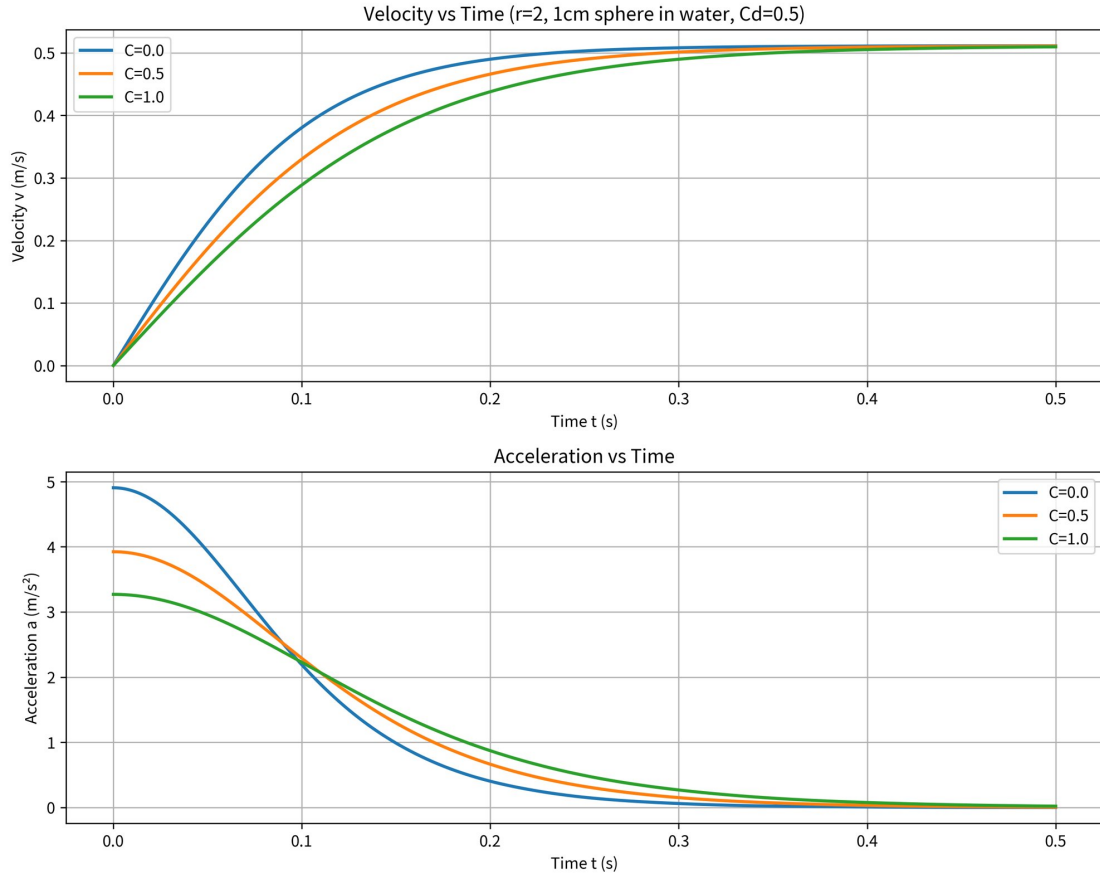


Figure 8: Velocity (top) and acceleration (bottom) versus time for a 1 cm-scale body in water ( $\rho_m = 1000 \text{ kg m}^{-3}$ ,  $\rho_o = 2000 \text{ kg m}^{-3}$ ,  $C_d = 0.5$ ). Initial C-family accelerations match the analytical predictions exactly:  $C = 0 \rightarrow 4.905 \text{ m s}^{-2}$ ,  $C = 0.5 \rightarrow 3.924 \text{ m s}^{-2}$ , and  $C = 1 \rightarrow 3.270 \text{ m s}^{-2}$ . Clear geometry-dependent separation exists during the first  $\sim 60\text{--}100 \text{ ms}$  before drag progressively collapses the branches toward terminal evolution.

The early-time interval is emphasised because it isolates geometry-coupling behaviour before

accumulated drag and resistance progressively collapse distinct acceleration branches toward shared terminal evolution.

### 8.3. Existing Literature Anchors

McKee and Czarnecki (2019) report buoyant-rise initial-acceleration measurements for light spheres in water, and find that the observed accelerations are reproduced only when the participating-medium-load renormalisation  $(\rho_o + 0.5\rho_m)V$  is applied to the effective inertia. This is exactly the  $C = 0.5$  sphere branch of the C-family. Their measurement therefore stands as a positive published anchor for one specific branch of the framework. The  $C = 0$  column produces  $|a/g| > 1$  throughout the buoyant-rise regime ( $r < 1$ ), which contradicts observation: bounded buoyant rise does not exceed  $g$  in magnitude. McKee and Czarnecki’s data require the sphere branch  $C = 0.5$  specifically. The experimental gap that this framework’s flagship test is designed to fill is clean  $\rho_o \approx 2\rho_m$  initial-acceleration data for cylinder- $\perp$ -axis ( $C = 1$ ) and capsule (intermediate  $C$ ) bodies; the sphere branch is already supported.

### 8.4. Validation and Failure Criteria

The C-family validation programme returns a failure signal — the geometry-aware general law and the C-family structure of classical added-mass theory are challenged together — if any of the following hold robustly across multiple clean experiments:

- **F1.** Intermediate-density unconstrained initial acceleration ( $r \approx 2$ ) consistently matches  $a = g/2$  ( $C = 0$ , no medium participation) for cylinder-class bodies even when added-mass effects are properly accounted for, contradicting both the  $C = 1$  prediction and the broader added-mass literature.
- **F2.** Shape-controlled tests show no systematic difference between sphere, capsule, and cylinder initial accelerations at matched density, contradicting the geometry-dependent C-family structure.
- **F3.** Buoyant rise of light objects ( $r \ll 1$ ) consistently produces  $|a/g| > 1$  in the early-time window, in line with strict object-normalisation and against the bounded prediction.
- **F4.** Near-equilibrium ( $r \approx 1$ ) or saturation ( $r \rightarrow 0$ ,  $r \rightarrow \infty$ ) regimes deviate systematically from  $g\chi$ .

If early-time acceleration measurements at fixed density ratio  $r$  show no reproducible geometry-dependent separation beyond known uncertainty bounds, the central geometry-coupling interpretation of the C-family would be substantially weakened.

The programme returns a positive signal — the geometry-aware general law and the ValerieX organisation are validated together — if the inverse holds: cylinder- $\perp$ -axis initial accelerations track  $g\chi$  ( $C = 1$ ), sphere initial accelerations track the  $C = 0.5$  branch, capsule bodies trace intermediate values along the predicted  $C(L/D)$  curve,  $|a/g| < 1$  holds robustly across the full range of finite densities, and the §8 predictions match measurements within combined experimental and added-mass uncertainty.

Apollo 15 / Galileo equivalence (vacuum limit,  $\rho_m \rightarrow 0$ ) is already established and is not a C-family discriminator: in the vacuum limit the participating medium load  $C\rho_m$  vanishes for every  $C$  and all branches collapse to  $a = g$ . The C-family validation lives at intermediate density and finite  $\rho_m$ .

Stated bluntly: ValerieX is materially weakened if early-time accelerations at intermediate density show no geometry-dependent separation along the predicted C-family branches, or if measured acceleration in the unconstrained regime systematically deviates from  $g\chi$  after drag closure

is properly accounted for. The framework's testability lives in these two conditions.

The framework is therefore operationally falsifiable rather than purely interpretive (Figure 9).

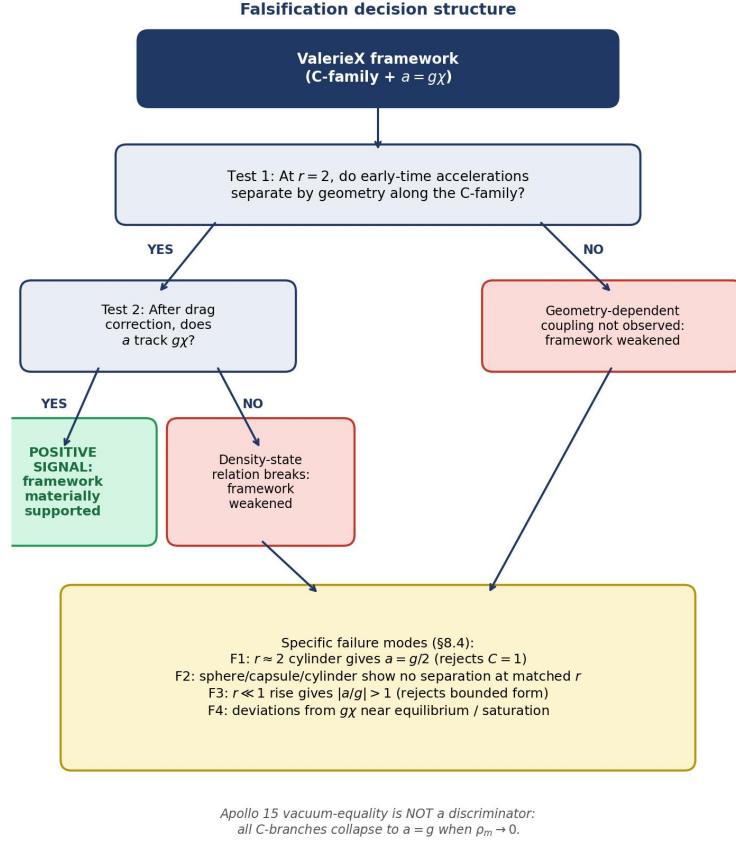


Figure 9: Logical falsification structure for the ValerieX framework. The framework is materially supported if early-time geometry-dependent acceleration branches emerge systematically along the C-family at  $r = 2$  (sphere  $\sim C = 0.5$ , capsule along the  $C(L/D)$  curve, cylinder  $\sim C = 1$ ) and if the resulting acceleration scaling follows the density-state relation  $a = g\chi$  after drag correction. Failure at either node weakens the framework. Analytical decision structure; the experimental tests of §9 implement these conditions.

### 8.5. Motion-Engine Reading: Early-Time Geometry Separation at Fixed Density Ratio

The flagship test of §8.2 is the experimental signature of the motion-engine identity. At fixed density ratio  $r = \rho_o/\rho_m = 2$ , ValerieX predicts that early-time acceleration is not determined by density contrast alone in a realised finite medium. Density contrast supplies the available drive; geometry sets the coupling branch through  $C$ . The geometry-aware general law at  $r = 2$  reduces to

$$\frac{a}{g} = \frac{1}{2 + C},$$

giving the following ordering by geometry:

- Sphere ( $C = 0.5$ ):  $a/g = 0.4 \approx 3.92 \text{ m s}^{-2}$ ;
- Capsule ( $0.5 < C < 1$ ):  $0.333 < a/g < 0.4$ , with the  $L/D$  dependence given by the prolate-spheroid curve of §6.4;

- Cylinder  $\perp$  axis ( $C = 1$ ):  $a/g = 0.333 \approx 3.27 \text{ m s}^{-2}$ .

The motion-engine prediction is then direct:

*At identical density ratio, identical volume, identical medium, and identical release conditions, early-time acceleration should order by coupling geometry: sphere fastest, capsule intermediate, cylinder slowest.*

This is not a contradiction of classical added-mass theory; it is ValerieX’s motion-engine reading of it. The novelty is that the same observable result is interpreted as density-drive plus geometry-dependent coupling, rather than as a sum of separate force categories. The capsule  $C(L/D)$  curve of §6.4 — which predicts a continuous monotonic rise of  $C$  from 0.5 toward 1 as cylindrical-section aspect ratio increases — converts the binary sphere-vs-cylinder ordering into a continuous-parameter falsification target for the same motion-engine identity. McKee and Czarnecki (2019) provide the existing positive published anchor for the  $C = 0.5$  sphere branch; the targeted  $r = 2$  measurements with paired sphere–capsule–cylinder bodies fill the experimental gap on the  $C = 1$  cylinder  $\perp$  axis branch and the capsule continuum between them.

## 9. Experimental Protocol Summary

This section consolidates the practical laboratory protocol developed in full in Volume IV. The C-family validation tests, in order of decisive power for the geometry-dependent coupling structure, are: (1) intermediate-density acceleration test at  $r = 2$ ; (2) sphere–cylinder–capsule geometry test; (3) constrained / supported / unconstrained regime-transition tests; and (4) an exploratory torsion configuration recorded as a regime-classification investigation only (not a C-family discriminator). The first three are the falsifiable core of the manual.

### 9.1. General Laboratory Rules

#### 9.1.1. Identify the regime first

Before any measurement, classify the test condition: constrained (blocked by rigid surface — surface force / scale reading), supported (held from above, pathway open below — tension / torsion / suspension signal), or unconstrained (pathway open, no support — acceleration / motion). The same density contrast can produce different measured signatures depending on whether motion is blocked, held, or free; every experiment must state its regime before interpretation.

#### 9.1.2. Drag-timescale estimation (Reynolds-based)

For a body of characteristic length  $L$  moving at velocity  $v$  in a medium of density  $\rho_m$  and dynamic viscosity  $\eta$ ,  $\text{Re} = \rho_m v L / \eta$ . As an order-of-magnitude estimate, the velocity at which drag equals 10% of the net driving force is  $v_{10} \approx \sqrt{0.2|\rho_o - \rho_m|gL/(C_d\rho_m)}$ . For a 4 cm sphere in water at  $\rho_o = 2\rho_m$ , this gives  $v_{10} \approx 0.2\text{--}0.3 \text{ m s}^{-1}$  and  $\text{Re} \approx 8000\text{--}12000$ . For a body released from rest under the  $C = 1$  prediction  $a \approx g/3$ , the time to reach  $v_{10}$  is  $t_{10} \approx 60\text{--}90 \text{ ms}$  for centimetre-scale bodies in water. Compute  $t_{10}$  for each test geometry and density pair, and trim the fitting window to  $t \lesssim t_{10}/2$  to keep the drag correction below 5% during the fit.

#### 9.1.3. Early-time measurement window

The fit window is bounded below by release-transient timescales (typically 5–20 ms) and above by  $t_{10}/2$ . For centimetre-scale bodies in water at  $r = 2$  the resulting window is approximately 20–40 ms. Within this window, fit position to  $y(t) = y_0 + v_0 t + \frac{1}{2}at^2$  and extract  $a$  from the quadratic coefficient; verify that the residuals do not show systematic curvature. Frame rate

$\geq 240$  fps gives 5–10 frames within a 20–40 ms window — acceptable but tight; 1000 fps gives 20–40 frames and materially improves the uncertainty on  $a$ . Sensitivity of the fitted acceleration to window length should be tested and reported.

#### 9.1.4. Release mechanism

Release the body fully submerged, not at the surface (eliminates surface-tension transients and air-cavity entrainment); use a matched-density holder that opens cleanly without imparting angular momentum (an electromagnetic gate or a split sleeve held closed by a pin pulled vertically clear of the path is acceptable; squeezing or rotating mechanisms are not); ensure the body is at rest at the moment of release (settle for  $\geq 60$  s after any disturbance); place the body so that the camera frame captures the full fit window before the body crosses any wall standoff threshold ( $\geq 5$  body diameters from any wall). Discard the first 5–20 ms after release from the fit and verify with high-frame-rate playback that the body is moving cleanly without rotation before the fit window begins.

#### 9.1.5. Density-measurement tolerances

Target  $\pm 1\%$  on each of  $\rho_o$  and  $\rho_m$ , propagated as a combined  $\pm 2\%$  on  $r$  and corresponding  $\pm 1\%$  on the predicted  $a$ . Measure  $\rho_m$  by hydrometer or by mass-balance of a calibrated displacement vessel ( $\pm 0.5\%$ ); measure  $\rho_o$  per body by mass and by water-displacement volume ( $\pm 1\%$ ) — do not assume the bulk material density of the printer feedstock or moulded plastic. Record temperature with each density measurement (water density varies  $\approx 0.05\%$  per  $^\circ\text{C}$  near room temperature). Reject any body whose individually measured density deviates from the target by more than  $1.5\%$ .

#### 9.1.6. Imaging resolution at $r = 2$

The two discrimination targets at  $r = 2$  differ by an order of magnitude in their imaging-precision requirements. The  $C = 0$  vs  $C = 1$  separation ( $\sim 0.167g$ ,  $\sim 1.63 \text{ m s}^{-2}$ ) corresponds to a position difference of approximately 0.7 mm at the upper edge of a 30 ms fitting window. This is comfortably resolvable on commodity 240 fps imaging with millimetre-scale calibration. The  $C = 0.5$  vs  $C = 1$  separation ( $\sim 0.067g$ ) corresponds to only about 0.3 mm at  $t = 30$  ms; resolving this requires frame rate  $\geq 1000$  fps, calibration at  $\leq 0.2$  mm per pixel, rigid camera mounting, sub-pixel centroid tracking, and confirmed sub-millimetre repeatability of the release mechanism.

#### 9.1.7. Composite Uncertainty Budget

This subsection composes the dominant systematics into a propagated uncertainty on the fitted early-time acceleration  $a$  at  $r = 2$ , so that experimental claims and discrimination margins can be stated against an explicit budget. The reference values below are for centimetre-scale bodies in water at  $\rho_o = 2\rho_m$  using 1000 fps imaging with 0.2 mm/pixel calibration; they should be re-evaluated for any other configuration. Each source is to be propagated through to the fitted  $a/g$  and reported alongside the measurement, not assumed at the apparatus level.

Source	Reference contribution to fitted $a$	Cross-ref
Density tolerance on $\rho_o, \rho_m$ (each $\pm 1\%$ )	$\leq 1\%$ on the predicted $a$ ( $\approx 0.03 \text{ m s}^{-2}$ ); affects the prediction line, not the measurement	§9.1.5
Release transient (first 5–20 ms discarded)	$\leq 1\%$ on $a$ ( $\approx 0.04 \text{ m s}^{-2}$ ) for trials passing no-rotation playback check	§9.1.4
Orientation drift during fit window (cylinder $\perp$ axis)	$\leq 2\%$ on $a$ ( $\approx 0.07 \text{ m s}^{-2}$ ) when trials with $> 5$ drift are rejected	—
Wall and finite-container effects (standoff $\geq 5$ body diameters)	$\leq 3\%$ on $a$ ( $\approx 0.10 \text{ m s}^{-2}$ ) at minimum standoff; reducing with larger standoff	Brennen 1982 §3.3
Drag onset within fit window ( $t \lesssim t_{10}/2$ )	$\leq 2\%$ on $a$ ( $\approx 0.07 \text{ m s}^{-2}$ ) given the sub-window stability check	§9.1.2, §9.1.3
Tracking resolution (1000 fps, sub-pixel centroid, $\sigma_y \approx 0.05 \text{ mm}$ )	$\approx 1.5\%$ on $a$ ( $\approx 0.05 \text{ m s}^{-2}$ ) over a 30 ms fit window	§9.1.6
Frame-rate / time-base calibration	Negligible at $\leq 10^{-4}$ relative	—

Treating the per-trial sources as approximately independent and combining in quadrature, the single-trial uncertainty on  $a$  at  $r = 2$  with cylinder  $\perp$  axis bodies and 1000 fps imaging is approximately

$$\sigma_a \text{ (single trial)} \approx \sqrt{0.04^2 + 0.07^2 + 0.10^2 + 0.07^2 + 0.05^2} \text{ m s}^{-2} \approx 0.15 \text{ m s}^{-2},$$

corresponding to  $\approx 4\text{--}5\%$  of the  $C = 1$  prediction ( $a = 3.27 \text{ m s}^{-2}$ ) and  $\approx 4\%$  of the  $C = 0.5$  prediction ( $a = 3.92 \text{ m s}^{-2}$ ). With the minimum-evidence requirement of  $\geq 10$  trials per condition (§9.7), the standard error of the mean reduces this to  $\approx 1.5\%$  per branch.

Resolvability against the C-family separations:

- $C = 0$  vs  $C = 1$  separation ( $\approx 1.63 \text{ m s}^{-2}$ ) is resolved at  $> 10\sigma$  on the SEM at 1000 fps and  $> 5\sigma$  at 240 fps; this is the primary flagship discriminator and is comfortably accessible on commodity equipment.
- $C = 0.5$  vs  $C = 1$  separation ( $\approx 0.65 \text{ m s}^{-2}$ ) is resolved at  $\approx 4\text{--}5\sigma$  on the SEM at 1000 fps with the budget above; this is tight, and the geometry-controlled discriminator depends on holding each source within the reference contributions stated.
- Continuous-parameter capsule  $C(L/D)$  test (§6.4) requires the same imaging chain as the  $C = 0.5$  vs  $C = 1$  separation; the predicted ordering  $a_{\text{sphere}}(r) > a_{\text{capsule}}(r) > a_{\text{cylinder}}(r)$  at  $r > 1$  is detectable provided per-shape SEM remains below half the smallest predicted increment between adjacent  $L/D$  points.

**Failure mode.** If the per-trial uncertainty exceeds 5% of  $a$  — for example because frame rate is below 1000 fps, calibration is coarser than 0.2 mm/pixel, wall standoff is insufficient, the release-transient discard window is too short, or orientation control is inadequate — the  $C = 0.5$  vs  $C = 1$  sphere/cylinder discriminator and the capsule continuum become inconclusive. The  $C = 0$  vs  $C = 1$  flagship discriminator remains accessible at lower precision (240 fps, 1 mm calibration), with the trade-off noted in §9.1.6. Any experimental claim must report both the budgeted contributions used and the per-trial and SEM uncertainties achieved, so that the resolvability of the relevant separation can be assessed independently of the central values.

## 9.2. Experiment 1 — Intermediate-Density Flagship Test

Aqueous medium with controlled density (water + NaCl/glycerol,  $\rho_m \approx 1000\text{--}1500 \text{ kg m}^{-3}$ ) and machined or 3D-printed test bodies of matched density  $\rho_o = 2\rho_m$ . Release from rest in a tank large enough to suppress wall effects (lateral and bottom standoff  $\geq 5$  body diameters; release depth such that the body crosses  $\geq 3$  diameters before any wall interaction). Capture motion with high-speed video ( $\geq 240$  fps) or an onboard accelerometer; fit the initial slope of  $v(t)$  over the first 20–100 ms before drag dominates. Run paired sphere and cylinder bodies of identical volume and density to test the geometry-aware extension simultaneously.

Result	Interpretation
$a \approx g/3$	C-family validation: matches $C = 1$ (cylinder $\perp$ axis) branch
$a \approx g/2$	C-family validation: matches $C = 0$ (no medium participation) branch — challenges added-mass coupling
$a$ between $g/3$ and $g/2$	Indicates intermediate participation coefficient — within the C-family but between branches
inconsistent / noisy	Repeat with improved release, tracking, and controls

**Vacuum-limit control note.** Free-fall comparisons performed under near-vacuum conditions are not discriminators between the C-family branches. As  $\rho_m \rightarrow 0$  the participating medium load  $C\rho_m$  vanishes for any value of  $C$ , the medium’s viscous resistance also vanishes, and all branches collapse to  $a = g$ . Vacuum tests therefore serve as positive controls for the apparatus and for the saturation limit of the C-family, but cannot discriminate between competing predictions: the discrimination is intrinsically a finite-medium measurement at intermediate density and shape-controlled coupling.

## 9.3. Experiment 2 — Shape-Controlled C-Family Test

Same fluid, same  $\rho_o/\rho_m$ , same initial-acceleration measurement window. Predicted branches: cylinder  $\perp$  axis tracks  $C = 1$  ( $a = g\chi$ ); sphere tracks  $C = 0.5$ . Predicted gap at  $r = 2$  is approximately  $\Delta a \approx 0.067g$  ( $\sim 0.66 \text{ m s}^{-2}$ ) — well above experimental noise. The hemisphere-ended capsule extends the test to a continuous-parameter discriminator: by varying the cylindrical-section length while holding the cross-sectional radius and density fixed, a capsule sweeps the participation coefficient across the predicted range  $0.5 < C_{\text{capsule}} < 1$  (the  $C(L/D)$  curve of §6.4). Short capsules approach the sphere limit; long capsules approach the perpendicular-cylinder limit. Any monotonic capsule-length trend in early-time  $a/g$ , at fixed  $\rho_o$  and  $\rho_m$ , is direct evidence for the C-family structure and cannot be reproduced by a single fixed-coefficient model.

From the measured acceleration, fit the participation coefficient via  $C = [g(r - 1)/a] - r$ . Falsification: the C-family validation programme returns a failure signal — challenging both ValerieX and the classical added-mass theory it is consistent with — if sphere, capsule, and cylinder give no measurable separation; if the cylinder does not approach the  $C = 1$  branch; if the sphere does not separate toward the  $C = 0.5$  branch; or if the measured order is repeatedly opposite to prediction.

## 9.4. Experiments 3–5 — Regime-Transition Tests

Three regime-transition tests demonstrate the regime classification with everyday equipment. **Experiment 3** (co-free-fall zero-reading test): place a test mass on a digital scale inside a protective drop box, drop the box, and record the scale reading during fall. Expected: scale reading goes to near-zero during the unconstrained-regime phase and returns when the system lands and re-enters the constrained regime. The  $\chi$ -drive itself is unchanged; the regime change

is the cause of the reading change. **Experiment 4** (surface vs suspension): record the same object on a digital scale (constrained-regime reading: realised weight) and hung from a spring scale (supported-regime reading: transmitted density-state drive / tension). The numerical readings can be close; under ValerieX they record structurally different quantities. **Experiment 5** (accelerating-frame transition): track the continuous decrease of scale reading as a system transitions from rest (constrained) toward free fall (unconstrained), demonstrating that the available  $\chi$ -drive is invariant under the transition while the realised expression changes with pathway condition.

### 9.5. Experiment 6 — Exploratory Torsion Configuration

This investigation is presented as an exploratory regime-classification observation rather than as a quantitative test or competing-prediction discriminator. Under the regime classification of §7, suspended torsion-balance configurations occupy the supported regime — a structural classification that follows from the operational criterion of §7.3. No quantitative density-state competing prediction for the magnitude or scaling of the observed Cavendish torque is asserted in this paper; whether such a prediction can be developed is treated as an open question (V2 §5.5 and Appendix A). The cross-method consistency of measured  $G$  across torsion-balance, free-fall, atom-interferometry, lunar laser ranging, satellite-orbit, and Earth-tide determinations (Gillies, 1997, and subsequent precision-G literature) is acknowledged as genuine empirical confirmation of the conventional Newtonian gravitational interpretation, and is not contested. The configuration variations recorded in V4 §9.3–§9.5 are exploratory variations of interest that would accompany any future quantitative density-state development of the supported-regime torque, not falsifiable tests in the present formulation. The constrained-regime configuration is structurally difficult to realise without losing the torsion measurement itself: if the test masses are supported from below by a rigid platform that takes their weight, the torsion fibre no longer carries net vertical load and the angular degree of freedom against which torque is read is not equivalent to the standard configuration.

### 9.6. Experiment 7 — Medium-Substitution Discriminator

This test examines whether the early-time acceleration in the unconstrained regime is set by the density-state contrast ( $\rho_o - \rho_m$ ) between object and medium alone, or whether non-density properties of the medium (viscosity, compressibility, dielectric constant, molecular structure) contribute an additional, independently observable term over and above that contrast. At fixed  $r = 2$  and fixed geometry (cylinder  $\perp$  axis,  $C = 1$ ), the C-family early-time prediction depends only on the density ratio  $r$  and the geometry coefficient  $C$ , so it is invariant under any change of medium that holds  $\rho_m$  fixed.

Use two media of identical density  $\rho_m \approx 1000 \text{ kg m}^{-3}$  but different composition: pure water and an aqueous glycerol/NaCl mixture tuned to the same  $\rho_m$  within  $\pm 0.1\%$ . Use the identical  $r = 2$  cylinder. Predicted  $a = g/3 \approx 3.269 \text{ m s}^{-2}$ , identical in both media. Measured difference within  $\pm 1\%$  ( $\leq 0.05 \text{ m s}^{-2}$ ) supports the C-family early-time prediction under these conditions; a systematic difference correlated with non-density medium properties would challenge density-contrast sufficiency.

### 9.7. Minimum Evidence Standard

For a result to count as meaningful: at least 10 repeats per condition; density measurements recorded; temperature recorded; raw video retained; early-time fitting method stated; drag-dominated late-time data not used as initial acceleration; regime declared before interpretation; error bars shown; null or failed results included; mean, standard deviation, and confidence intervals reported for all measured accelerations; any systematic drift between trials investigated and



documented.

9.8. Recommended Build Order

**Stage 1** — Easy demonstrations (regime logic): surface vs suspension; co-free-fall scale drop; accelerating-frame transition. Stage 1 also includes the high-drag shuttlecock drop (§4.3.6), which holds  $\chi$  near saturation while drag dominates the realised motion — an accessible phone-video illustration of the drive/resistance separation requiring no tank or precision release; feather-versus-synthetic comparison probes  $C_d$  at fixed  $\chi$ . **Stage 2** — Core discriminator: intermediate-density  $r = 2$  test (the  $C = 1$  bounded branch against the  $C = 0$  strict object-normalised limit). **Stage 3** — Geometry discriminator: sphere vs capsule vs cylinder, including the continuous  $C(L/D)$  capsule sweep. **Stage 4** — Density-contrast independence: medium-substitution test at the same  $r = 2$  cylinder. **Stage 5** — Exploratory torsion configuration (optional, regime-classification only).

9.9. Pass/Fail Summary

Test	Validation supports the framework if...	Validation challenges the framework if...
$r = 2$ discriminator	Measured $a$ approaches $g/3$ ( $C = 1$ ) for cylinder $\perp$ axis bodies; tracks predicted C-family branch for each geometry	Repeatedly approaches $g/2$ ( $C = 0$ ) for cylinder $\perp$ axis bodies — would also challenge classical added-mass theory
Sphere / cylinder / capsule	Fitted $C$ separates by shape; capsule traces continuous interpolation $0.5 < C < 1$ along predicted $C(L/D)$	No repeatable shape dependence — would challenge classical added-mass theory broadly
Co-free-fall	Scale reading collapses during free fall	Scale reading remains unchanged
Surface / suspension	Same $\chi$ gives different regime signature	Regime has no measurable relevance
Torsion configuration	Exploratory only — no falsifiable density-state competing prediction asserted	Cross-method $G$ consistency (Gillies, 1997) confirms the conventional interpretation
Medium-substitution	Same $a$ within $\pm 1\%$ ( $\leq 0.05\text{ m s}^{-2}$ ) across two media of identical $\rho_m$ but different composition	Systematic, repeatable difference correlated with non-density medium properties

10. Scope and Limitations

The present formulation applies specifically to vertical motion in a surrounding environment and to the role of density-state disequilibrium in organising the available vertical-motion response.

The scope is deliberately restricted to phenomena that can be directly observed, measured, and repeated under everyday or accessible laboratory conditions: rest, rise, fall, flotation, buoyant motion, terminal behaviour in real media, and intermediate-density and shape-controlled discrimination regimes. Phenomena that are not directly accessible to repeatable everyday measurement — orbital dynamics, planetary mechanics, satellite motion, interplanetary trajectories, gravitational lensing, cosmological-scale structure, and the precision- $G$  measurement programme — lie

outside this scope and are neither addressed nor displaced by the framework. Vertical direction in ValerieX is the local resolution direction set by the gradient structure of the surrounding medium; it is not asserted as a universal cosmological direction. The framework is offered as an organisation of the vertical-motion observables that any reader can in principle reproduce.

### 10.1. What the Framework Treats

- Equilibrium and neutral suspension.
- Rise and fall in media.
- Vacuum-limit free-fall behaviour.
- Reinterpretation of weight, buoyancy, and gravitational response under the regime classification.
- Terminal behaviour through realised-motion constraint.
- Geometry-aware realised acceleration through participating medium load.
- Thermal, acoustic, and pressure-driven motion through density-state modulation.

### 10.2. What the Framework Does Not Yet Provide

- A first-principles derivation of  $g$  (treated as observed, not derived).
- Cosmological-scale extensions (out of scope).
- Quantitative reproduction of precision- $G$  measurements within the density-state framework (named explicitly as future work).
- The full transient drag-coupled ODE is now stated in Appendix B; it composes the C-family early-time drive with the bluff-body terminal velocity through one closed equation. The core C-family law remains the early-time drive at  $t = 0^+$ , before drag closure dominates. The present consolidated paper deliberately isolates early-time behaviour so that density contrast and geometry-dependent coupling can be tested cleanly before terminal effects dominate.
- CFD-grade capsule  $C(L/D)$  predictions: the §6.4 prolate-spheroid mapping is a first-order approximation; a CFD or boundary-element computation that handles the hemispherical end-caps explicitly would refine the curve, particularly at small  $L/D$  where end-cap effects are largest in proportion.

### 10.3. Honest Statement of Position

The paper does not reject existing measurements. Weighing-scale readings, torsion-balance deflections, atom-interferometric phase shifts, and precision determinations of  $G$  are all real, reproducible observables, and the paper takes them as such. The paper does not claim that ValerieX has quantitatively reproduced the numerical value of  $G$ ; that is named explicitly as future work. The paper does not reinterpret cosmological-scale phenomena, strongly non-inertial systems, or configurations whose pathway condition is itself ambiguous. The paper does not derive the environmental scale  $g$  from first principles.

What the paper does is supply (i) a symmetry-based derivation of the bounded contrast variable  $\chi$  and Valerie's Law; (ii) a regime classification of terrestrial laboratory configurations; (iii) the geometry-aware C-family extension and its capsule continuous discriminator; and (iv) a falsifiable experimental programme — the C-family validation tests at  $r = 2$  and across paired sphere–capsule–cylinder geometries — by which the structural claims could be tested. These are stated as boundaries of the present formulation rather than as defects. Each represents a defined

route for further development.

#### 10.4. Natural Extensions and Adjacent Phenomena

The framework is scope-limited to vertical motion in a surrounding medium under everyday and laboratory conditions. Several phenomena are adjacent to this scope: their structural form follows the same drive–coupling–resistance–pathway organisation, but quantitative extension lies outside the present formulation. They are listed here to clarify the framework’s reach without claim of completeness.

**Oscillatory and pendulum-like motion under small disequilibrium.** The near-equilibrium linear regime of §4.3.2 generalises to linear restoring behaviour for an object slightly displaced from its suspension layer in a stratified medium. The natural extension is a Brunt–Väisälä-like internal-gravity-wave structure read in density-state terms; quantitative development requires explicit treatment of the medium gradient  $\rho_m(z)$  and is left to subsequent work.

**Multi-body and stratified configurations.** Cartesian-diver behaviour, density-stratified columns, and density-current flows are conceptually expressions of the same density-state drive in non-uniform  $\rho_m(z)$ . The Cartesian diver in particular is a clean pedagogical case: Boyle’s Law modulates  $\rho_o$  inside the diver, and the regime transition from buoyant rise ( $\chi < 0$ ) through neutral suspension ( $\chi = 0$ ) to sinking ( $\chi > 0$ ) is observable in real time as the surrounding  $\rho_m$  is held fixed and  $\rho_o$  is varied by external pressure.

**Acoustic levitation and Chladni patterns.** §4.3.4 indicates that acoustic forcing enters Valerie’s Law as a time-varying  $\rho_m(t)$ . The natural extension treats standing-wave levitation as time-averaged  $\chi$ -minimisation at pressure nodes, with Chladni and Faraday patterns (Chladni 1787; Faraday 1831; Kundt 1866) read as the mode structure of the time-averaged density-state field. Quantitative development requires the time-averaged form of Valerie’s Law under an oscillating  $\rho_m$  and is not undertaken here.

**Compressible and rarefied-gas regimes.** ValerieX takes  $\rho_o$  and  $\rho_m$  as state variables. In compressible flows where  $\rho$  varies on the timescale of the motion itself, the framework requires augmentation by an equation of state. The transition to molecular flow at very low  $\rho_m$ , where the continuum description fails, lies outside the continuum scope adopted here.

**Non-vertical and anisotropic-medium motion.** Vertical direction in ValerieX is set locally by the gradient structure of the surrounding medium. Cases where the medium gradient is itself oriented (sloping density layers, atmospheric thermals, oceanic density currents) admit a natural extension via projection onto the local gradient direction. Genuine horizontal motion in an isotropic medium is not addressed by the framework and is correctly described by direct electromagnetic and contact interactions (cf. §2.4, Axiom 7).

**Cosmological, orbital, and precision- $G$  regimes.** Explicitly outside scope (§10.2). The framework does not assert that the  $\chi$ -based reading extends to gravitational interactions where no surrounding medium is identifiable. The cross-method consistency of measured  $G$  across torsion-balance, free-fall, atom-interferometry, lunar laser ranging, satellite-orbit, and Earth-tide determinations (Gillies 1997) is acknowledged as genuine empirical confirmation of the conventional Newtonian gravitational interpretation in those regimes.

These extensions share the same drive–coupling–resistance–pathway organisation that governs the in-scope phenomena. Where the analogous structure can be identified, the framework’s reading extends; where it cannot, the framework does not apply. The boundaries are stated openly rather than implied, so that future development can proceed on clear ground.

## 11. Conclusion

ValerieX is presented as a symmetry-based, motion-first reorganisation of classical buoyancy and added-mass behaviour, grounded in density-state disequilibrium and governed by Valerie’s Law,

$$a = g \cdot \frac{\rho_o - \rho_m}{\rho_o + \rho_m} = g\chi.$$

From a minimal ontological base, the framework derives a bounded, antisymmetric, scale-neutral law of available vertical motion; proves the uniqueness of  $\chi$  as the lowest-degree rational function meeting the four foundational conditions; and characterises every higher-degree solution as  $\chi$  multiplied by an even, scale-neutral correction. The framework recovers the principal observables of vertical motion — rest, rise, fall, vacuum free fall, weight-response, buoyancy-response, and terminal behaviour — from one law plus medium participation rather than from a stack of separate primitive force terms.

Geometry enters through the participation coefficient  $C$ , and the bounded form is recovered exactly at the  $C = 1$  branch of the recognised classical added-mass family — the participating-medium-load coefficient for a circular cylinder moving perpendicular to its axis in inviscid potential flow (Brennen, 1982; Lamb, 1932; Kelvin, 1871). The terrestrial scale  $g = 9.80665 \text{ m s}^{-2}$  (NIST CODATA) is treated as the observed ceiling of realised vertical particle acceleration under full contrast, interpreted as the pathway-availability ceiling at which available motion is fully realised. Realised motion is organised by a regime classification with three operationally distinct regimes — constrained, supported, and unconstrained — each defined by a single directly observable pathway condition.

Three experimental routes isolate early-time coupling behaviour and discriminate the C-family branches: the intermediate-density unconstrained measurement at  $\rho_o = 2\rho_m$ , where the C-family predicts  $a = g/3$  ( $C = 1$ , cylinder  $\perp$  axis),  $a = 2g/5$  ( $C = 0.5$ , sphere), and  $a = g/2$  ( $C = 0$ , strict object-normalised limit); shape-controlled measurements with paired sphere–capsule–cylinder bodies, with capsule bodies tracing the continuous prolate-spheroid-derived  $C(L/D)$  curve; and the medium-substitution discriminator that probes density-contrast sufficiency at fixed  $r$  and geometry. McKee and Czarnecki (2019) provide a positive published anchor for the  $C = 0.5$  sphere branch; the experimental gap to be filled is clean  $\rho_o = 2\rho_m$  initial-acceleration data for the cylinder  $\perp$  axis ( $C = 1$ ) branch and for the continuous-parameter capsule curve. The exploratory torsion configuration is recorded as a regime-classification investigation only and does not assert a quantitative density-state competing prediction for the Cavendish torque; the cross-method consistency of measured  $G$  across multiple independent methods (Gillies, 1997) is acknowledged as genuine empirical confirmation of the conventional Newtonian gravitational interpretation.

The intent of this paper is to set the reorganisation out cleanly, anchor it in observation and the established literature, and invite collaborative engagement with its structural contributions and its open questions. The framework is scope-limited throughout to vertical-motion phenomena that can be directly observed, measured, and reproduced in everyday and laboratory conditions. It does not extend to orbital, planetary, or cosmological scales;  $g$  is treated as observed, not derived; and vertical direction is treated as locally defined by the surrounding medium rather than as a universal absolute. Volumes I–IV remain the canonical technical record and are referenced throughout this paper as the supporting package for readers wishing to consult the full detail. Appendices A and B record the formal characterisation of higher-degree rational solutions and the full transient drag-coupled ODE, respectively, both of which extend the technical content of the main sections without altering the foundational framework.

Each clause is an empirical claim that can be tested against observation, against the classical interpretation, or against the experimental programme set out in §9 and developed in full in

Volume IV. The framework is offered for collaborative engagement on those terms.

The novelty is not the replacement of classical equations but their reorganisation: vertical motion read through a single relational density-state structure, with the geometry-sensitive early-time discrimination programme of §8 as the experimental anchor on which the structural claim stands or falls.

Figure 10 provides a condensed overview of the complete ValerieX organisational structure.

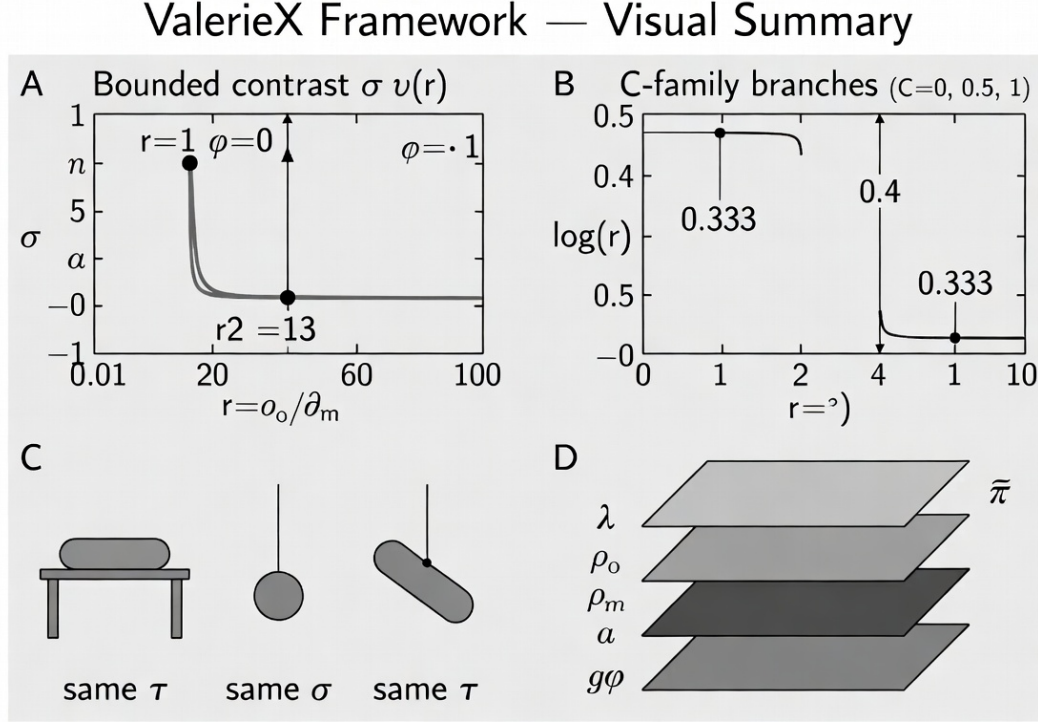


Figure 10: ValerieX visual summary: bounded density-state contrast, geometry-dependent coupling through the C-family, pathway-regime expression, and the EM-conditioned material substrate.

ValerieX is therefore presented as a bounded phenomenological motion framework operating within experimentally accessible fluid-mechanical regimes, rather than as a complete replacement for established gravitational, relativistic, or quantum theories.

*ValerieX does not reject the classical equations. It identifies a single motion-engine structure beneath them and invites the work of testing whether that structure holds.*

## A. Higher-Degree Rational Solutions and Their Exclusion by Minimal Sufficiency

The General Theorem of §3.4 states that every rational solution of the four foundational conditions takes the form  $f = \chi \cdot R$ , where  $R$  is even under  $(\rho_o \leftrightarrow \rho_m)$  and homogeneous of degree zero. This appendix characterises  $R$  explicitly and shows where the empirical content of the minimal-sufficiency axiom (Axiom 6) lies.

### A.1. Reduction to a function of $\chi^2$

Any even, scale-neutral rational function of  $(\rho_o, \rho_m)$  reduces to a rational function of the dimensionless ratio  $\chi^2 = [(\rho_o - \rho_m)/(\rho_o + \rho_m)]^2$ . Setting  $s = \rho_o + \rho_m$  and  $d = \rho_o - \rho_m$ , every even homogeneous-degree-0 rational form can be written as a polynomial in  $d^2/s^2 = \chi^2$ , up to common-factor cancellation. Therefore  $R = R(\chi^2)$ .

### A.2. Boundedness and saturation constraints on $R$

For  $f = \chi R(\chi^2)$  to satisfy the four foundational conditions:

- Antisymmetry holds automatically since  $\chi$  is odd and  $R(\chi^2)$  is even.
- Scale-neutrality holds automatically.
- Equilibrium ( $f = 0$  at  $\chi = 0$ ) requires  $R(0)$  finite.
- Boundedness ( $|f| < 1$  strictly, with  $|f| \rightarrow 1$  only at the singular vacuum limits) requires  $R(1) = 1$  and  $|\chi R(\chi^2)| < 1$  throughout  $|\chi| < 1$ .

### A.3. The one-parameter family

The simplest non-trivial  $R$  consistent with these constraints is

$$R(\chi^2) = 1 + \kappa(\chi^2 - 1), \quad 0 \leq \kappa \leq 1,$$

which gives  $R(0) = 1 - \kappa$ ,  $R(1) = 1$  (saturation preserved), and the candidate solution

$$f_\kappa(\chi) = (1 - \kappa)\chi + \kappa\chi^3.$$

At  $\kappa = 0$  the unadorned  $\chi$  is recovered (the ValerieX form). At  $\kappa = 1$  the candidate reduces to  $f = \chi^3$ , which is bounded, antisymmetric, scale-neutral, and saturates correctly at  $\chi = \pm 1$ . Higher polynomial  $R$  generates families  $f = \chi R(\chi^2)$  with additional parameters and additional inflexion structure on the  $\chi$ -axis. All such solutions are mathematically admissible under the first four conditions; none is required.

### A.4. Empirical content of the minimal-sufficiency selection

Axiom 6 selects  $\kappa = 0$  — the linear form  $a = g\chi$  across the full range  $-1 < \chi < 1$  — because no axiom and no observation in the present formulation requires  $\kappa \neq 0$ . This selection is empirically falsifiable. Any systematic deviation from the linear  $a/\chi$  relation across the C-family branches, after geometry coupling and drag are properly accounted for, would constitute evidence for  $\kappa > 0$  and for higher-degree structure beyond the minimal form.

The flagship  $r = 2$  measurement of §8 already samples one specific value ( $|\chi| = 1/3$ ). A programme of measurements at multiple  $|\chi|$  — for example  $r = 1.2, 1.5, 2, 3, 5$  (corresponding to  $|\chi| \approx 0.091, 0.20, 0.33, 0.50, 0.67$ ) using the same cylinder  $\perp$  axis bodies in the same medium-substitution geometry — would constrain  $\kappa$  directly. A null result across this range would close the empirical gap left by the minimal-sufficiency selection. A non-null result at any  $|\chi|$  would force ValerieX to abandon the linear form and adopt the appropriate  $f_\kappa(\chi)$ .

The minimal-sufficiency axiom is therefore not a stipulation against testing. It is a statement that, in the absence of evidence for additional structure, ValerieX takes the simplest admissible form — and identifies the measurements that would force it to abandon that form.

## B. Transient Drag-Coupled Motion: The Full ODE

The C-family acceleration law  $a = g(\rho_o - \rho_m)/(\rho_o + C\rho_m)$  supplies the early-time drive at  $t = 0^+$ . For finite times in a real medium, the full transient is governed by the drag-coupled ordinary differential equation

$$(\rho_o + C\rho_m)V\frac{dv}{dt} = Vg(\rho_o - \rho_m) - \frac{1}{2}\rho_m C_d A v|v|,$$

with initial condition  $v(0) = 0$ . The left-hand side carries the participating-medium-load coefficient of the C-family. The right-hand side carries the density-state drive (first term) and the bluff-body drag closure (second term, with the  $v|v|$  form preserving signed motion through reversal points).

### B.1. Limiting cases

- *At  $v = 0$ :*  $dv/dt = a_0 \equiv g(\rho_o - \rho_m)/(\rho_o + C\rho_m)$ . The C-family early-time law of §4.2 is recovered identically.
- *At terminal velocity ( $dv/dt = 0$ ):*  $v_t = \sqrt{2Vg|\Delta\rho|/(\rho_m C_d A)}$  — identical to the bluff-body terminal velocity of §4.3.3.
- *In the vacuum limit  $\rho_m \rightarrow 0$ :* the LHS reduces to  $\rho_o V dv/dt$  and the RHS to  $Vg\rho_o$  for any  $v$ , giving  $dv/dt = g$  unconditionally. The universal-fall regime of §5.2 is recovered as a structural collapse: medium participation, viscous resistance, and inertial drag all vanish together.

### B.2. Non-dimensional form

Setting  $v = v_t u$  and  $t = \tau_0 \tau$  with  $\tau_0 = v_t/a_0$ , the ODE reduces to

$$\frac{du}{d\tau} = 1 - u|u|,$$

with  $u(0) = 0$ . The solution for  $u \geq 0$  is  $u(\tau) = \tanh(\tau)$ , which interpolates monotonically between the early-time linear regime  $u \approx \tau$  (i.e.  $v \approx a_0 t$ , the C-family law) and the late-time steady state  $u \rightarrow 1$  (i.e.  $v \rightarrow v_t$ , the realised terminal velocity). The full transient is parameter-free in this form: a single hyperbolic-tangent curve carries the full motion from rest to terminal regime in every C-family configuration, with  $a_0$  and  $v_t$  as the only system-specific scales.

### B.3. Calibration of the early-time fit window

The early-time fit window of §9.1.3 (20–40 ms for centimetre-scale bodies in water at  $r = 2$ ) corresponds to  $\tau \leq 0.15$  for representative parameters: with  $a_0 \approx g/3 \approx 3.27 \text{ m s}^{-2}$  and  $v_t \approx 0.7 \text{ m s}^{-1}$  for a 1 cm sphere in water at  $r = 2$ ,  $\tau_0 \approx 0.21 \text{ s}$ . At  $\tau = 0.15$  the fractional deviation of  $u$  from the linear approximation  $u \approx \tau$  is

$$\frac{\tau - \tanh \tau}{\tau} \approx \frac{\tau^2}{3} \approx 0.75\%,$$

well below the per-trial uncertainty budget of §9.1.7. The position-based fit  $\frac{1}{2}a_0 t^2$  has even smaller deviation from the exact form  $\int \tanh d\tau = \ln \cosh \tau$  in this window. The fit window of §9.1.3 is therefore safely within the linear-velocity approximation, and the C-family early-time prediction can be extracted cleanly without transient-form corrections.

## B.4. Compositional structure

The transient ODE composes both halves of the ValerieX motion engine into one closed equation: the symmetry-derived drive  $Vg(\rho_o - \rho_m)$  on the right, the participating-medium-load  $(\rho_o + C\rho_m)V$  on the left, and the medium-set bluff-body resistance closing the late-time regime. No additional physical content is introduced. The drive is supplied by density-state disequilibrium; the coupling is set by geometry through  $C$ ; the resistance is set by the medium through  $C_d$ . The same three-role decomposition that organises Valerie's Law also organises the transient form. The ODE is its time-resolved expression.

## References

- Archimedes (c. 250 BCE). *On Floating Bodies*. English translation in Heath, T. L. (ed.), *The Works of Archimedes*, Cambridge University Press.
- American Chemical Society. *Middle School Chemistry, Chapter 3 Lesson 6: Temperature Affects Density*.  
<https://www.acs.org/middleschoolchemistry/lessonplans/chapter3/lesson6.html>
- Batchelor, G. K. (1967). *An Introduction to Fluid Dynamics*. Cambridge University Press.
- Bernoulli, D. (1738). *Hydrodynamica, sive de viribus et motibus fluidorum commentarii*. Strasbourg.
- Boyle, R. (1662). *New Experiments Physico-Mechanical, Touching the Spring of the Air and Its Effects*. Oxford.
- Brennen, C. E. (1982). *A Review of Added Mass and Fluid Inertial Forces*. Report CR 82.010, Naval Civil Engineering Laboratory, Port Hueneme, CA.
- Cavendish, H. (1798). Experiments to determine the density of the Earth. *Philosophical Transactions of the Royal Society of London* 88, 469–526.
- Chladni, E. F. F. (1787). *Entdeckungen über die Theorie des Klanges*. Leipzig: Weidmanns Erben und Reich.
- Euler, L. (1757). Principes généraux du mouvement des fluides. *Mémoires de l'Académie des Sciences de Berlin* 11, 274–315.
- Faraday, M. (1831). On a peculiar class of acoustical figures and on certain forms assumed by groups of particles upon vibrating elastic surfaces. *Philosophical Transactions of the Royal Society* 121, 299–340.
- Galilei, G. (1638). *Discorsi e dimostrazioni matematiche intorno a due nuove scienze*. Leiden: Elsevier.
- Gillies, G. T. (1997). The Newtonian gravitational constant: recent measurements and related studies. *Reports on Progress in Physics* 60(2), 151–225.
- Helmholtz, H. von (1863). *Die Lehre von den Tonempfindungen als physiologische Grundlage für die Theorie der Musik*. Braunschweig: Vieweg.
- Kelvin, Lord (W. Thomson) (1871). Hydrokinetic solutions and observations. *Philosophical Magazine* 42(281), 362–377.
- Kundt, A. (1866). Über eine neue Art Akustischer Staubfiguren. *Annalen der Physik* 127, 497–523.
- Lamb, H. (1932). *Hydrodynamics*, 6th ed. Cambridge University Press.
- Landau, L. D. and Lifshitz, E. M. (1959). *Fluid Mechanics*. Oxford: Pergamon Press.
- Levin, Y., da Silveira, F. L. and Rizzato, F. B. (2006). Electromagnetic braking: a simple



- quantitative model. *American Journal of Physics* 74(9), 815–817.
- McKee, K. and Czarnecki, A. (2019). Acceleration due to buoyancy and mass renormalization. *American Journal of Physics* 87(3), 165–170.
- Newton, I. (1687). *Philosophiæ Naturalis Principia Mathematica*. London: Royal Society.
- NIST (2019). CODATA recommended value: standard acceleration of gravity,  $g_n = 9.80665 \text{ m s}^{-2}$ . <https://physics.nist.gov/cgi-bin/cuu/Value?gn>
- OpenStax. *University Physics Volume 1, Chapter 17: Sound*.  
<https://openstax.org/books/university-physics-volume-1/pages/17-1-sound-waves>
- Parkyn, N. (2026a). *ValerieX (VXXX) — Volume I. A Symmetry-Based Reorganisation of Classical Buoyancy and Added-Mass Behaviour: Theory and Derivation*.
- Parkyn, N. (2026b). *ValerieX (VXXX) — Volume II. Regime Classification and Experimental Discrimination*.
- Parkyn, N. (2026c). *ValerieX (VXXX) — Volume III. Computational Modelling, Discriminators, and Figure Framework*.
- Parkyn, N. (2026d). *ValerieX (VXXX) — Volume IV. Experimental Protocol and Laboratory Manual*.
- Peastrel, M., Lynch, R. and Armenti, A. (1980). Terminal velocity of a shuttlecock in vertical fall. *American Journal of Physics* 48(7), 511–513.
- Rayleigh, J. W. S. (1877). *The Theory of Sound*, Vol. 1–2. London: Macmillan.
- Reynolds, O. (1883). An experimental investigation of the circumstances which determine whether the motion of water shall be direct or sinuous. *Philosophical Transactions of the Royal Society* 174, 935–982.
- Schlichting, H. and Gersten, K. (2017). *Boundary-Layer Theory*, 9th ed. Berlin: Springer.
- Scott, D. (1971). *Apollo 15 Mission Report*. NASA MSC-05161, Houston, TX.
- Hammer-and-feather demonstration, 2 August 1971.
- Stokes, G. G. (1851). On the effect of the internal friction of fluids on the motion of pendulums. *Transactions of the Cambridge Philosophical Society* 9, 8–106.
- U.S. Department of Energy. *DOE Explains... The Electromagnetic Force*.  
<https://www.energy.gov/science/doe-explainsthe-electromagnetic-force>
- U.S. Department of Energy. *DOE Explains... Quantum Mechanics*.  
<https://www.energy.gov/science/doe-explainsquantum-mechanics>
- White, F. M. (2011). *Fluid Mechanics*, 7th ed. New York: McGraw-Hill.